

# GALAXY DISTANCES IN THE NEARBY UNIVERSE: CORRECTIONS FOR PECULIAR MOTIONS

CHRISTIAN MARINONI<sup>1,2</sup>, PIERLUIGI MONACO<sup>3</sup>, GIULIANO GIURICIN<sup>1,2</sup>, AND BARBARA COSTANTINI<sup>1,2</sup>

<sup>1</sup> Dipartimento di Astronomia, Università di Trieste, via Tiepolo 11, 34131 Trieste, Italy

<sup>2</sup> SISSA, via Beirut 4, 34013 - Trieste, Italy,

<sup>3</sup> Institute of Astronomy, Madingley Road, Cambridge, CB3 0HA, UK

e-mail: marinoni@mizar.sissa.it; monaco@ast.cam.ac.uk; giuricin@newton.sissa.it;

barbara@newton.sissa.it

## ABSTRACT

By correcting the redshift–dependent distances for peculiar motions through some peculiar velocity field models, we recover the true distances of an extensive, all-sky sample of nearby galaxies ( $\sim 6400$  galaxies with recession velocities  $cz < 5500 \text{ km s}^{-1}$ ), which is complete up to the apparent limiting blue magnitude  $B = 14$  mag. Relying on available catalogs of galaxy groups, we treat  $\sim 2700$  objects as members of galaxy groups and the remaining objects as field galaxies.

We invert the derived redshift–distance relations to estimate distances for field galaxies and groups and we overcome the ambiguity inherent to the triple-valued zones by using Tully–Fisher relations calibrated on suitably defined samples of galaxies having distances predicted by peculiar velocity models.

We use two independent approaches to modeling the peculiar velocity field: i) a cluster dipole reconstruction scheme that we modify with the inclusion of a local model of Virgocentric-infall; ii) a multi–attractor model fitted to the Mark II and Mark III catalogs of galaxy peculiar velocities. In the multi–attractor model we assume that the velocity field is generated by a few prominent gravitational sources (Virgo cluster, "Great Attractor", Perseus–Pisces Supercluster, and Shapley supercluster).

We discuss differences in the results coming out from different velocity models and from different Mark II and Mark III data subsets. In particular, according to Mark III data the Great Attractor appears to have a smaller influence on local dynamics than previously believed, whereas the Perseus–Pisces and Shapley superclusters acquire a specific dynamical role. Remarkably, the Shapley structure, which is found to account for nearly half the peculiar motion of the Local Group, is placed by Mark III data closer to the zone of avoidance with respect to its optical position. On the other hand, the modified cluster dipole model is characterized by relatively small flows towards the Great Attractor and the Shapley supercluster, together with a large Virgocentric infall.

Our multi–attractor model based on Mark III data favors a cosmological density parameter  $\Omega_0 \sim 0.5$  (irrespective of a biasing factor of order unity).

The use of different peculiar velocity field models allows us to check to what extent differences in current views on cosmic flows affect the recovering of galaxy distances. We find that differences among distance estimates are less pronounced in the  $\sim 2000 - 4000 \text{ km s}^{-1}$  distance range than at larger or smaller distances. In the last regions these differences have a serious impact on the 3D maps of the galaxy distribution and on the local galaxy density — on small scales ( $< 1 \text{ Mpc}$ ) —, which is a crucial parameter being used in statistical studies of environmental effects on the properties of nearby galaxies.

*Subject headings:* galaxies: distances and redshifts — galaxies: clusters: general — cosmology: large-scale structure of universe

## 1 INTRODUCTION

The determination of galaxy distances is one of the most fundamental problem in extragalactic astronomy. In particular, galaxy distances allow us to map the three-dimensional (3D) distribution of galaxies and hence to evaluate the local galaxy density, which is an important characteristics of the galaxy environment.

In many previous studies which rely only on the two-dimensional (2D) projection of galaxies on the sky (see, e.g., Lahav (1987) for all-sky 2D optical maps of bright galaxies), a local galaxy density parameter is defined in terms of galaxy counts over a sky area which are statistically corrected for projection effects. With the advent of large surveys of galaxy redshifts and well-selected galaxy

catalogs, it has become possible to map the spatial distribution of galaxies and hence to construct a 3D definition of the local galaxy density.

Optical galaxy samples are more suitable for mapping the galaxy density field on relatively small scales than IRAS-selected galaxy samples, which have been frequently used as tracers of the density field on large scales up to a recession velocity  $cz \sim 20000 \text{ km s}^{-1}$  (e.g., Rowan-Robinson et al., 1990; Kaiser et al., 1991; Strauss et al., 1992a,b; Fisher et al., 1995). The latter samples have the advantage that they are homogeneously selected and penetrate to lower galactic latitudes because IRAS fluxes are much less impeded by Galactic extinction. But the IRAS galaxy samples have the serious drawback that they do not

include the early-type galaxies (because of their little dust content and star formation), which usually lie in the densest regions of clusters and superclusters. Furthermore, the density field traced by IRAS galaxies is noisy nearby, because of the sparseness of the samples and because IRAS fluxes are much less linked with galaxy mass than optical fluxes. Therefore, in the following we shall focus on all-sky optical galaxy samples.

The magnitude-limited Revised Shapley-Ames (RSA) Catalog of Bright Galaxies (Sandage & Tamman, 1981), which contains the first large compilation of redshift data for bright galaxies across the entire sky, was used by Yahil, Sandage & Tamman (1980) to delineate the 3D-density field of galaxies in the Local Supercluster (LS). The structures of the LS region have been comprehensively described and named by Tully & Fisher (1987). The former author intended to include all nearby galaxies with systemic recession velocities  $cz < 3000 \text{ km s}^{-1}$  (2367 objects) in his Nearby Galaxies Catalog (Tully, 1988a, hereafter NBG), which is a combination of the RSA catalog and a diameter-limited sample of late-type and fainter galaxies found in an all-sky HI survey made principally by Fisher & Tully (1981) and Reif et al. (1982). In the NBG catalog, which is complete up to the corrected blue total magnitude  $B_T \sim 12 \text{ mag}$  (although it extends to fainter magnitudes), the distances of all non-cluster galaxies have been estimated on the basis of their redshifts, with an assumed Hubble constant  $H_0 = 75 \text{ km s}^{-1} \text{ Mpc}^{-1}$ , whereas the galaxy members of systems with relatively high velocity dispersion have been given a distance consistent with the mean redshift of the system. The important fact that redshifts are not equivalent to distances because galaxies have peculiar motions (i.e. deviations from the pure Hubble flow) is simply taken into account in the NBG catalog through the Virgocentric retardation model described by Tully & Shaya (1984), in which the authors assume that the Milky Way is retarded by  $300 \text{ km s}^{-1}$  from the pure Hubble flow by the mass of the Virgo cluster. Defining the local galaxy density on the basis of his NBG catalog, Tully (1988b) incorporated corrections for the catalog incompleteness at large distances.

Later, similar quantifications of the local galaxy density, based on the NBG catalog data, have been exploited in statistical analyses of environmental effects on some properties of LS galaxies such as the frequency of bars (Giuricin et al., 1993), the classification of spiral arms (Giuricin et al., 1994), the frequency of active galactic nuclei (LINER and Seyfert objects) selected from optical spectroscopic surveys (Monaco et al., 1994), and the bulge-to-disk light ratio (Giuricin et al., 1995).

In an effort of going beyond the LS, Hudson (1993a,b; 1994a,b) assembled an extensive galaxy sample from a merging of the diameter-limited northern UGC catalog (Nilson, 1973) and the diameter-limited southern ESO catalog (Lauberts, 1982; Lauberts & Valentijn, 1989). He took into account the fairly large incompleteness in redshift of his sample as a function of angular diameter and position on the sky, by applying statistical corrections,

which allowed him to reconstruct the density field of optical galaxies to a depth of  $cz = 8000 \text{ km s}^{-1}$ .

The Lyon-Meudon Extragalactic Database (LEDA), which collects and homogenizes several data for all the galaxies of the main optical catalogues, such as the catalogs UGC (Nilson, 1973), ESO (Lauberts, 1982, Lauberts & Valentijn, 1989), CGCG (Zwicky et al., 1961-1968), and ESGC (Corwin & Skiff, 1998, in preparation), allows the extraction of an all-sky galaxy sample which has properties of completeness and is deep enough to probe the galaxy field significantly beyond the LS. In particular, Garcia et al. (1993) extracted a magnitude-limited sample which covers all the sky and contains 6392 galaxies having recession velocities  $cz < 5500 \text{ km s}^{-1}$ . Although different optical catalogs are characterized by different limits of completeness in apparent magnitude or angular diameter, the above-mentioned galaxy sample was found to be substantially complete up to its limiting corrected total blue magnitude  $B_T = 14 \text{ mag}$  (for galactic latitudes  $|b| > 20^\circ$ ) (Garcia et al., 1993). The authors tabulated several parameters for each galaxy, such as the morphological type, the maximum velocity rotation deduced from the deprojected 21-cm hydrogen line width, the de Vaucouleurs' luminosity index, the distance modulus, the corrected angular sizes and total blue magnitudes. The authors derived the last two quantities by transforming the original raw data to the standard system of the RC3 catalog (de Vaucouleurs et al., 1991) and by applying corrections for Galactic extinction, internal extinction, and K-dimming. Only for the few galaxies which lack magnitude measures, the values of  $B_T$  are rough estimates derived from their diameters through a mean magnitude-diameter relation. The tabulated distance modulus was a weighted mean derived from the combination of redshift-distances (with  $H_0 = 75 \text{ km s}^{-1} \text{ Mpc}^{-1}$ ) and redshift-independent distances obtained from distance indicators (DIs), i.e. from a Tully-Fisher (TF) relation (which relates the absolute magnitude  $M_B$  to the logarithmic maximum rotation velocity  $\log V_m$ ) and a luminosity-luminosity index relation. In particular, the authors used the former kind of distances alone for the farthest galaxies (with  $cz > 1500 \text{ km s}^{-1}$ ) and the latter kind alone for the few nearest objects (with  $cz < 500 \text{ km s}^{-1}$ ).

Group assignments for the galaxies of this sample have been provided by Garcia (1983). She employed two 3D methods of group identification, the percolation or *friends of friends* method proposed by Huchra & Geller (1982) and the hierarchical clustering method (Materne, 1978; Tully, 1980, 1987). The latter method gave, on average, smaller groups than the former. The adopted final catalog of groups was defined as that one which includes only groups (as well as galaxy members) common to the two catalogs. Accordingly, 3381 objects are field galaxies. Of the remaining grouped objects, 2703 galaxies are members of 485 systems with at least three members; most of them are groups which contain less than 10 members, and 13 systems have more than 20 members (among which the clusters Virgo, Centaurus, Perseus).

A somewhat different approach to the construction of a large and deep sample of optical galaxies with good completeness in redshift was followed by Santiago et al. (1995). Their "Optical Redshift Survey" is a redshift survey of an optical galaxy sample which contains 8266 galaxies with known redshift. This sample consists of two largely overlapping subsamples (which are limited in magnitude and in diameter, respectively) drawn from the catalogs UGC, ESO, ESGC. The authors selected their own sample according to the raw (observed) magnitudes and diameters (rather than the corresponding corrected values) and then quantified the effects of Galactic extinction (as well as random and systematic errors) on the optical density field. Redshift-distances were used in general, but the members of rich clusters were placed at each cluster's center. Probing the density field at large depth (up to  $cz = 8000 \text{ km s}^{-1}$ ) requires much care in the derivation of appropriate selection functions, which quantify the loss of galaxies due to magnitude or diameter limits or other observational selection effects. Taking into account possible non-uniformities in galaxy sampling, the authors attempted to match the original three catalogs from which their sample was drawn, by using separate selection functions (Santiago et al., 1996).

The reliability of the distances given in all above-mentioned galaxy samples (and hence of the resulting galaxy density field) is weakened by the fact that simple redshift-distances are in general adopted with no corrections (or no adequate corrections) for the peculiar motions which are due to inhomogeneous mass distribution and which prevent redshift to scale linearly with distance.

In the present paper we propose to recover the true distances of a sample of nearby galaxies by treating adequately the effects of peculiar velocities of galaxies. As shown in a forthcoming paper (Marinoni et al., 1998b), in which the resulting 3D galaxy density field is presented and local galaxy density parameters (corresponding to various smoothing scales) are discussed, corrections of galaxy distances for peculiar motions appear to have a large impact on the values of the aforementioned parameters on small scales (i.e. on  $< 1 \text{ Mpc}$  scale) and, hence, on the characterization of the environment (see §6).

For our purpose, we take the above-mentioned complete sample extracted from LEDA (Garcia et al., 1993; Garcia, 1993), for which all galaxy data as well as group assignments are available in the literature. Thus, we limit ourselves to the nearby universe (within  $cz = 5500 \text{ km s}^{-1}$ ), where the peculiar velocity field is best known and no large corrections for galaxy sample incompleteness are required. However, the galaxy sample considered is deep enough to cover interesting regions of prominent overdensities, such as the "Great Attractor" (GA) region and the Perseus-Pisces supercluster.

The study of the peculiar velocity field resulting from a proper analysis of large redshift-distance samples (i.e., samples of galaxies having both redshift and redshift-independent distance estimates) has acquired a well-established role in the cosmological context (e.g., for test-

ing the gravitational instability paradigm for the origin of large-scale structure, for deducing the relative distributions of luminous and dark matter, and for constraining the value of the cosmological density parameter  $\Omega_0$ ; see, e.g., the reviews by Dekel, 1994, and Strauss & Willick, 1995).

In general, peculiar velocity analyses proceed along two main lines of research. One can turn a distribution of galaxies or galaxy systems with known redshifts into a smoothed mass-density field (under the linear approximation of the gravitational instability theory) and then predict from it the peculiar velocity field, e.g., by means of the "dipole analysis". Despite the complexity of these studies, the velocity vector of the Local Group (LG) with respect to the reference frame defined by the cosmic microwave background (CMB) ( $v_{LG} \sim 630 \text{ km s}^{-1}$  towards  $l \sim 277^\circ$  and  $b \sim 30^\circ$  (Lubin & Vilella, 1986; Kogut et al., 1993)) has been approximately reconstructed in terms of the gravitational acceleration exerted by various populations of extragalactic objects (e.g., the references cited in Kolokotronis et al., 1996).

Alternatively, one can face the problem of deriving the true matter distribution from the observed peculiar velocity field, e.g. using few-parameter toy models or the non-parametric POTENT method developed by Bertschinger & Dekel (1989).

In this paper, following the second kind of approach, we attempt to correct the Hubble flow for peculiar motions by means of two basic independent approaches to modeling the velocity field in the nearby universe: i) a modified cluster dipole model, which is Branchini & Plionis' (1996, hereafter BP96) optical cluster dipole reconstruction scheme that we modify by including a local model of the Virgo-centric infall in the LS region. We regard the cluster dipole model as a typical approach in which the peculiar velocity field is self-consistently derived through iteration techniques from the redshifts and positions of a sample of objects. ii) a multi-attractor model, which we take as an example of a parametric toy model which is fitted to catalogs of peculiar velocities. In the multi-attractor model we assume that the velocity field is generated by a few prominent gravitational sources (Virgo cluster, Great Attractor, Perseus-Pisces Supercluster, Shapley concentration).

We construct these models relying on the various data subsets contained in the Mark II and Mark III catalogs of peculiar velocities of galaxies. In particular, the Mark III catalog (Willick et al., 1997a), which is the most comprehensive homogenized catalog of peculiar velocities available today, is a merging of several data sets of spiral and elliptical galaxies.

Through these peculiar velocity field models we provide homogeneous estimates of distances for our galaxy sample. Moreover, we can evaluate to what extent differences in current views on the peculiar motions affect the recovering of galaxy distances and, hence, the 3D maps of galaxy distribution.

The outline of our paper is as follows. In §2 we describe the properties of the Mark II and Mark III catalogs which

are relevant to our velocity field models. In §3 we present our two basic approaches to modeling the peculiar velocity field and we discuss the results relative to different data sets. In §4 we address the inversion of the redshift-distance relation and, in particular, the ambiguity inherent to the triple-valued zones of this relation. We attempt to solve this problem using blue TF relations calibrated on suitably defined samples of galaxies having distances predicted by velocity field models. In §5, outlining some basic differences among the velocity field models, we discuss the resulting sets of galaxy distances. In our conclusions (see §6) we mention some developments of peculiar velocity studies and focus on the effects of our galaxy distance corrections on the determination of the 3D galaxy density field.

Throughout, the Hubble constant is  $75 h \text{ km s}^{-1} \text{ Mpc}^{-1}$ . In general, distances are expressed in velocity units ( $\text{km s}^{-1}$ ).

## 2 THE MARK II AND MARK III PECULIAR VELOCITY CATALOGS

Our modeling of the peculiar velocity field is substantially based on several data subsets contained in the Mark III catalog of radial peculiar velocities (Willick et al., 1995, 1996, 1997a). This is a homogenized database of redshift-independent distance estimates obtained using the revised Faber-Jacson ( $D_n - \sigma$ ) relation for early-type galaxies and both the forward and inverse TF relations for spirals. Input data come from different samples of galaxies, but the inferred galaxy distances are the result of an accurate analysis which carefully takes into account differences in the observational selection criteria, in the methods of measurement, in the TF calibration techniques, in statistical bias effects. The uniformity of corrected data is ensured through transformations onto a common system and through a mutually consistent TF calibration for the samples of spirals. The  $D_n - \sigma$ -inferred distances for early-type galaxies are rescaled in order to match the distance scale of spirals.

This catalog is the current evolution of the previous Mark II catalog compiled by Burstein (1989), which is a merged set of 1184 galaxies grouped into 704 objects (single galaxies, groups, and clusters). Of these galaxies, the ellipticals (E) and lenticulars (S0) come from a combinations of the dataset used by Lyndell-Bell et al. (1988) in their analysis of the GA region and those by other authors (Lucey & Carter, 1988; Faber et al., 1989; Dressler & Faber, 1990). The spiral sample consists of the Aaronson "good" and "fair" field spirals (see Faber & Burstein, 1988, and Aaronson et al., 1989, for the definitions), the Aaronson cluster spirals, the spirals of de Vaucouleurs & Peters (1984). In some cases we present results derived from the Mark II data alone in order to emphasize the differences between Mark II and Mark III data.

With nearly 3400 galaxies, the Mark III catalog, which includes Mark II data with some improvements, is almost three times bigger than its predecessor and has a better space coverage. It contains new samples of spirals which

cover sky regions poorly mapped in Mark II. Maps of the spatial distribution of the various subsamples, which probe different regions of the sky, are presented by Kollatt et al. (1996). In our analysis we use the following different subsamples, avoiding the possibility that the same object be included in different samples:

1. the E/S0 galaxy sample (Lynden-Bell et al. 1988; Faber et al. 1989; Lucey & Carter, 1988; Dressler & Faber, 1990). It includes 544 galaxies grouped into 249 objects which map the GA region.
2. the HMCL cluster sample of spirals (Han & Mould, 1992) with 36 objects.
3. the WCF group sample of spirals (Willick, 1991; Courteau, 1992; Courteau et al., 1993; Courteau, 1996) which contains 65 groups of galaxies covering the Perseus-Pisces region.
4. the MAT data set of spirals (Mathewson, Ford & Buchorn, 1992) with 277 groups selected in the southern hemisphere.
5. the A82 spiral sample (Aaronson et al., 1982) as revised by Tormen & Burstein (1995). Of the 359 galaxies contained in the sample, 222 have been grouped in 67 groups (Willick et al., 1996) and 137 are field galaxies.

The analysis of different data subsets allows us to test the stability of our final results against the particular subsample used. The whole data set, in which we take together spirals and ellipticals (which should trace the same velocity field) will help us to give more stringent constraints on our models than smaller subsamples would.

The accuracy of the peculiar velocities achieved in Mark III catalog is not only due to a careful homogenization of different data subsets and DIs for getting a uniform distance scale; it is also due to the new approach with which the authors treat sample selection (or calibration) effects, which typically enter in the calibration of the DI being used in flux-limited samples, and the inferred-distance effects, also called Malmquist bias, which typically enter when a calibrated DI is used to infer distances and hence peculiar velocities (e.g. Willick, 1994). Selection effects are due to the fact that a magnitude limit in the selection of the sample used for calibration at a fixed *true* distance (e.g., in a cluster) tilts the direct TF regression line ( $M_B$  versus  $\log V_m$ ) towards bright  $M_B$  at small values of  $\log V_m$ . The homogeneous part of the Malmquist bias arises from the space geometry in the sense that the inferred distance  $d$  underestimates the true distance  $r$  because it is more likely to have been scattered by errors from  $r > d$  rather than from  $r < d$ , the volume being  $\propto r^2$ . The inhomogeneous part of the Malmquist bias arises from number density fluctuations and tends to enhance systematically the inferred density perturbations.

Clearly, removing the overall Malmquist effect (known as inhomogeneous Malmquist bias), arising from both vol-

ume effects and density variations, is of fundamental importance to yield unbiased peculiar velocities. In the Mark III catalog this was done using smoothed density fields obtained from the IRAS 1.2 Jy redshift survey (Fisher et al., 1995), with the effect of peculiar velocities corrected for using linear theory (Yahil et al., 1991). The resulting field is expected to represent the general spiral density field on large scales.

Thus, besides the uncertainties inherent to DI calibration procedures, the Mark III distances rely also on a model-dependent reconstruction of the general density field from redshift data. Moreover, redshift limits in a sample modify the nature of the Malmquist bias corrections applied. It would be worse to neglect any correction for the Malmquist bias; but we have to take into account the possibility that further errors and systematic effects can affect the data. Therefore, in our analysis we increase the tabulated errors on distances by a factor of 3, according to D. Burstein's advices for the Mark II catalog.

For all the single objects we have taken the Malmquist-corrected forward TF distances, since this is the best approach to follow in our statistical analysis. Our approach belongs to the method I of the "method matrix" of peculiar velocity analysis illustrated in §5.2 of Strauss & Willick (1995). On the other hand, the forward TF distances of the spiral groups are fully corrected only for selection bias, because they are formed using redshift-space criteria and in this case it is selection bias rather than Malmquist bias which pertains. Residual Malmquist bias due to clustered structures still affects the data of spiral groups. Nevertheless, the grouping procedure reduce distance uncertainties by a factor  $N^{1/2}$ , if  $N$  is the number of grouped galaxies.

### 3 CORRECTING GALAXY DISTANCES THROUGH VELOCITY FIELD MODELS

At the low redshifts discussed in this paper the Hubble law,  $cz = H_0 r$ , is an excellent approximation in describing the Friedmann expansion of the universe. However, galaxies have motions above and beyond their Hubble recession velocities. Therefore, by combining the cosmological component of redshift with the peculiar one, the Hubble relation is modified to:

$$cz \approx H_0 r + [\mathbf{v}(\mathbf{r}) - \mathbf{v}(\mathbf{0})] \cdot \hat{\mathbf{r}} + \left[ \frac{\mathbf{v}(\mathbf{r}) \cdot \hat{\mathbf{r}} - \mathbf{v}(\mathbf{0}) \cdot \hat{\mathbf{r}}}{c} + \frac{(\mathbf{v}(\mathbf{0}) \cdot \hat{\mathbf{r}})(\mathbf{v}(\mathbf{r}) \cdot \hat{\mathbf{r}})}{c^2} \right] H_0 r - \frac{(\mathbf{v}(\mathbf{r}) \cdot \hat{\mathbf{r}})(\mathbf{v}(\mathbf{0}) \cdot \hat{\mathbf{r}})}{c} \quad (1)$$

where  $\hat{\mathbf{r}}$  is the unit vector towards the galaxy in question,  $\mathbf{v}(\mathbf{r})$  is the peculiar velocity of a galaxy at position  $\mathbf{r}$ , and  $\mathbf{v}(\mathbf{0})$  is the non-comoving velocity of the observer.

To first order approximation and in the Local Group rest frame, the distance of a galaxy (expressed in  $\text{km s}^{-1}$ ) can be written as:

$$r = cz - [\mathbf{v}(r, l, b) - \mathbf{v}(\mathbf{0})] \cdot \hat{\mathbf{r}} \quad (2)$$

where  $l$  and  $b$  are the galactic longitude and latitude.

Thus, with a peculiar velocity field model which describes point by point the function  $\mathbf{v}(r, l, b)$ , it is possible to correct the linear Hubble law in order to take into account peculiar motions. We rely on two basic approaches to modeling the peculiar velocity field. They are described below.

#### 3.1 The Modified Cluster Dipole Model

##### 3.1.1 The Model

We use the BP96 optical cluster dipole model as a basic predictive model of the peculiar velocity field. The BP96 reconstruction scheme of the 3D positions and peculiar velocities of galaxy clusters is based on the observed distribution of an optical cluster sample (with  $r \leq 25000 \text{ km s}^{-1}$ ) extracted from the Abell/ACO sample (Abell, 1958; Abell, Corwin & Olowin, 1989). Taking into account observational biases through an homogenization procedure and filling artificially the zone of avoidance with a simulated population of galaxies, BP96 obtained a statistically homogeneous all-sky sample of clusters.

Under some general and reasonable assumptions, e.g. that the peculiar velocities are caused by gravitational instability, that linear instability theory applies and that cluster density fluctuations are related to the mass density fluctuations by a constant linear biasing factor  $\delta_c(\mathbf{r}) = b_c \delta(\mathbf{r})$ , a simple relation between the peculiar velocity of a galaxy and the surrounding mass density field can be derived (cf Peebles, 1980):

$$\mathbf{v}(\mathbf{r}) = \frac{\beta}{4\pi} \int \delta(\mathbf{r}') \frac{\mathbf{r}' - \mathbf{r}}{|\mathbf{r}' - \mathbf{r}|^3} d^3\mathbf{r}', \quad (3)$$

where  $\delta(r) = [\rho(r) - \rho_b]/\rho_b$  is the density fluctuation about the mean background density  $\rho_b$  and  $\beta = \frac{f(\Omega_0)}{b_c} \sim \frac{\Omega_0^{0.6}}{b_c}$ .

Within the linear theory approximation, BP96 used an iterative reconstruction algorithm to remove redshift space distortions, recovering both the real space distribution of clusters and the field of peculiar velocities generated by this cluster distribution.

The resulting density and velocity fields clearly depend on an assumed value of  $\beta$ , which is not directly provided by the procedure itself. Nevertheless, this kind of analysis yields a resulting cluster 3D dipole pointing only  $\sim 10^\circ$  away from the CMB apex; therefore, comparing the reconstructed cluster dipole amplitude to the LG peculiar velocity (as inferred by the CMB dipole) BP96 estimated  $\beta \sim 0.21$ .

The model gives some important information (such as bulk flow amplitudes) on large scales, but we are interested in constructing an accurate picture of the velocity field and in recovering galaxy distances in the region which lies within about  $5500 \text{ km s}^{-1}$ .

Because of the heavy smoothing procedure used, the cluster density is not known with a good local resolution. In other words, local contributions to the velocity field such as those originating from the gravity of the Virgo cluster, which is not even included in the Abell/ACO

Fig. 1.— The plots show the radial components (in the CMB frame) of the smoothed velocity fields in the supergalactic plane  $SGX, SGY$  for the cluster dipole model by Branchini & Plionis (1996) (left) and for the cluster dipole model modified with the inclusion of a Virgocentric infall (right). The field is smoothed with a  $1500 \text{ km s}^{-1}$  Gaussian window and is normalized to  $\beta = 0.21$ . The arrows and the boldface arrows distinguish between incoming and outgoing objects. The contours correspond to the same radial peculiar velocity; contour spacing is  $100 \text{ km s}^{-1}$ , with the heavy contour marking 0. Regions of different radial peculiar velocities are also indicated by shading. The Local Group is at the center, the Great Attractor is on the left, Perseus-Pisces is on the right, and Coma is at the top. Coordinates are expressed in  $\text{km s}^{-1}$ .

cluster sample because of its large angular size, are not taken into account.

We have address this problem by merging the cluster dipole model with a simple model of the Virgocentric infall. In our model we assume that the Virgo mass is spherically symmetric and is radially distributed with a King density profile

$$\rho(r) = \rho_b \left[ 1 + A(1 + x^2)^{-1.5} \right] \quad (4)$$

where  $x = r/r_c$ ,  $r$  is the distance of a galaxy from the Virgo center,  $r_c$  is a smoothing length, and  $A$  is a normalization mass factor. Using eq. 3 we obtain

$$\mathbf{v}(\mathbf{r}) = -A\Omega^{0.6}rx^{-3} \left[ \ln(x + \sqrt{1+x^2}) - \frac{1}{\sqrt{1+x^2}} \right] \hat{\mathbf{r}}. \quad (5)$$

where  $\hat{\mathbf{r}}$  is the unit vector pointing outward Virgo; the parameter  $r_c$  plays the role of a smoothing length necessary for the linear theory to hold.

We evaluate the influence of the Virgo cluster on the dynamics of the LS by fitting the predictions of our modified cluster dipole model with the observed radial velocities of

a sample of nearby galaxies having redshift-independent distances.

In this fit we fix the coordinates of Virgo cluster at  $l = 284^\circ$ ,  $b = 74^\circ$ ,  $r = 1350 \text{ km s}^{-1}$  (Virgo distance) as in Faber & Burstein (1988), whereas we treat  $C = A\Omega^{0.6}$  and  $r_c$  as free parameters of the model. Necessary ingredients in the fitting procedure are the radial components of peculiar velocities as predicted by the model ( $v_i^{mod}$ ), the corresponding observed recession velocities ( $cz_i$ ) and the galaxy distances  $r_i$ . The model parameters are determined by means of a  $\chi^2$  minimization procedure; we minimize the quantity

$$\chi^2 = \sum_i \frac{[cz_i - cz_i^{mod}(r_i, \alpha_k)]^2}{\sigma_i^2} \quad (6)$$

where  $cz^{mod}$  is given by eq. 2 and depends on a number of model parameters  $\alpha_k$ . The quantity  $\sigma^2$  is the quadratic sum of the uncertainties in the redshift measures, errors in the predicted redshifts induced by distance uncertainties plus a term which describes noise in the velocity field, under the assumption that these errors are independent.

Fig. 2.— The plots show the velocity field in the CMB frame for the cluster dipole model (left) and the modified cluster dipole model (right). The vectors shown are projections of the 3D velocity field in the supergalactic plane  $SGX, SGY$ . The contours correspond to the same velocity vector modulus; contour spacing is  $100 \text{ km s}^{-1}$ , with the heavy contour marking  $100 \text{ km s}^{-1}$ . Regions of different peculiar velocities are also indicated by shading. The Local Group is at the center, the Great Attractor is on the left, Perseus-Pisces is on the right, and Coma is at the top. Coordinates are expressed in  $\text{km s}^{-1}$ .

The last term is a value of dispersion associated to non-linear and non-spherically symmetric motions of galaxies which lie around collapsed systems and for which our models fail to predict the true radial velocity. For the first term we assume the value of  $50 \text{ km s}^{-1}$ , for the last we adopt the value of  $200 \text{ km s}^{-1}$  (e.g., Strauss & Willick 1995). We estimate the formal  $1\sigma$  errors of the model parameters from the covariance matrix calculated at the point which minimizes eq. 6 in parameter space.

For this fit we choose the A82 spiral sample described in §2. These galaxies are distributed quite uniformly in space around the Virgo cluster and therefore they are suitable for studying the Virgo infall in detail. The forward TF relation used for estimating the distances of these galaxies has a *rms* scatter of  $\sigma = 0.47 \text{ mag}$  (Willick et al., 1997a). Specifically, we consider the 158 galaxies of the A82 sample which have distances smaller than  $3000 \text{ km s}^{-1}$ . This upper limit reflects the vanishing of Virgo gravitational influence at large distances. Moreover, the A82 sample is strongly incomplete at large distances, since it exhibits an abrupt reduction in the number of objects per unit redshift at  $cz_{\odot} = 3000 \text{ km s}^{-1}$ . This redshift limit affects the reliability of the inhomogeneous Malmquist bias corrections

for the 59 objects lying beyond that limit.

### 3.1.2 Model-fitting results

The resulting best-fitting parameters  $C = A\Omega^{0.6}$  and  $r_c$  ( $\text{km s}^{-1}$ ) are tabulated in Table 1 together with the value of  $\chi^2$  per degree of freedom, which measures the goodness of the fit, and the *rms* dispersion of model velocity residuals  $\sigma(cz)$  (in  $\text{km s}^{-1}$ ).

TABLE 1

THE BEST-FITTING PARAMETERS FOR THE MODIFIED CLUSTER DIPOLE MODEL.

$C$	$r_c$ ( $\text{km s}^{-1}$ )	$\chi^2/dof$	$\sigma(cz)$ ( $\text{km s}^{-1}$ )
$3.4 \pm 1.3$	$810 \pm 110$	0.97	404

Fig. 1 shows the smoothed radial velocity fields (in the supergalactic plane  $SGX, SGY$ ) of the BP96 cluster dipole model and our modified cluster dipole model. Fig. 2 shows the smoothed velocity fields in the supergalactic plane  $SGX, SGY$  for the same models.

Although the BP96 cluster dipole model suffers from

uncertainties in the relation between fluctuations in matter and light distributions (e.g the *linear biasing* assumption), from sample selection effects, and from the method used to fill artificially the Zone of Avoidance, the model fits fairly well the A82 data in the LS region. The model implies a scatter of  $\sigma(cz) = 485 \text{ km s}^{-1}$  (with  $\chi^2/dof = 1.44$ ) which can be compared with the value of  $\sigma(cz) = 554 \text{ km s}^{-1}$  (with  $\chi^2/dof = 2.14$ ) which one would obtain by fitting an unperturbed Hubble flow (in the CMB frame) to the same data.

The fit becomes even better if we add the perturbing presence of Virgo cluster (see the low values of  $\sigma(cz)$  and  $\chi^2/dof$  listed in Table 1). From our best fit we infer that the LG has a Virgo infall velocity equal to  $v = 440 \pm 180$ . This value is larger than those quoted recently by several authors for whom the Virgo infall is not a major source of the velocity field in the LS, in disagreement with earlier contentions (see Han & Mould, 1990 for a summary table). In recent years, a large Virgo infall amplitude was also suggested by Tonry et al. (1992), who, applying the surface brightness fluctuation technique as DI for local ellipticals, found the value of  $v = 340 \pm 80 \text{ km s}^{-1}$ . On the other hand, from the analysis of the magnitudes of bright cluster galaxies in a way which is free of assumptions about motions in the LS, Gudehus (1995) found no significant evidence of a Virgo infall of the LG.

The too great an amplitude of LG infall velocity is not due to differences in the choice of observed Virgo redshift. It is instead likely due to the fact that the BP96 cluster dipole model generates on the LG a velocity vector (with projections along the supergalactic axes  $v_{SGX} = -225 \pm 61 \text{ km s}^{-1}$ ,  $v_{SGY} = 131 \pm 40 \text{ km s}^{-1}$ ,  $v_{SGZ} = -349 \pm 81 \text{ km s}^{-1}$ ) which has a lower component in the general direction of GA ( $v_{LG} = 285 \text{ km s}^{-1}$ ) than that predicted by other studies ( $v \sim 500 \text{ km s}^{-1}$ ; see, e.g., Faber & Burstein, 1988). So, in attempting to reproduce the local observed flow pattern, our fitting parameters have to compensate the underestimated GA infall of LG. This interpretation is consistent with the fact that the CMB anisotropy dipole has a component directed towards the Virgo cluster of  $v = 418 \pm 25 \text{ km s}^{-1}$  (see, e. g., the review by Davis & Peebles, 1983) and is supported by the fact that, by adding the Virgo mass contribution, we find a velocity component of the LG motion towards GA of  $v_{LG} = 558 \pm 170 \text{ km s}^{-1}$ , in good agreement with the value of  $v_{LG} = 535 \text{ km s}^{-1}$  obtained by Faber & Burstein (1988) with an independent model.

### 3.2 The Multi-Attractor model

#### 3.2.1 The Model

The GA model of the Seven Samurai, proposed by Lynden-Bell et al. (1988) and revised by Faber & Burstein (1988), is the current most popular phenomenological model of the large scale peculiar motions in the nearby universe. As claimed by several authors in the last years (e.g., Faber & Burstein, 1988; Han & Mould, 1990; Shimazaki & Okamura, 1992) and substantially confirmed by

a look at the mass density fields reconstructed through the application of the POTENT method to Mark II and Mark III data (e.g., Dekel et al. (1993) and Sigad et al. (1998), respectively), most of the local velocity field can be interpreted as being generated by few gravitational sources characterized by spherical symmetry. It is then sensible to describe the velocity field in term of a multi-attractor toy model dominated by spherically symmetric Virgocentric and GA-infalls. In this model we consider also the possible effect of other gravitational sources, such as the Perseus-Pisces Supercluster and the Shapley concentration.

This kind of model is an oversimplified *version of facts*, because it imposes a simple, spherical geometry on the adopted gravitational sources of a complex velocity field, which actually arises from a continuous field of asymmetric density fluctuations. Nevertheless, this model, which as yet has never been applied to Mark III data, is the most simple and statistically significant tool to analytically correct the Hubble law. As discussed below, the multi-attractor model yields predictions in satisfactory agreement with data and it is adequate for our purposes.

Instead of considering the gravitational instability paradigm, we use the infall model discussed by Regös & Geller (1989). In this model, based on the Friedmann solution, the motion of galaxies at a particular radius from the cluster center is approximated as the motion of a spherical mass shell, which follows the same gravitational equation of motion as the expansion factor of the universe. The shell can be treated as a Friedmann universe on its own; it is possible to define a formal Hubble constant and a formal cosmological density parameter  $\Omega$  for the shell. This infall model yields an implicit exact dependence, and an explicit approximate analytic expansion, for the peculiar velocity as a separable function of the present density contrast  $\langle \delta_0 \rangle$ , averaged inside a radius  $r$ , and the present cosmological parameter  $\Omega_0$ . In the range  $0.1 \leq \Omega_0 \leq 1$  this expansion can be written (Regös & Geller, 1989) as:

$$\begin{aligned} \mathbf{v}_p = -\mathbf{r} & \left[ \frac{1}{3} \Omega_0^{0.6} \langle \delta_0 \rangle - 0.063 \Omega_0^{0.68} \langle \delta_0 \rangle^2 + \right. \\ & + 0.027 \Omega_0^{0.71} \langle \delta_0 \rangle^3 - 0.015 \Omega_0^{0.72} \langle \delta_0 \rangle^4 + \\ & \left. + 0.01 \Omega_0^{0.75} \langle \delta_0 \rangle^5 \dots \dots \right] \end{aligned} \quad (7)$$

where the distance  $\mathbf{r}$  is expressed in  $\text{km s}^{-1}$ .

This series expansion provides convergence to the exact solution for  $\langle \delta_0 \rangle \leq 1 - 2$ . However because the linear term dominates in the peculiar velocity, the  $\Omega_0$  dependence of the exact solution is close to that of the linear approximation.

We approximate the total peculiar velocity as the sum of the components generated by the individual attractors. Assuming a King profile (eq. 4) for each attractor (so that infall velocities converge at the center of attracting mass), we build up a parameter toy model which is fitted to the various galaxy subsamples which are part of the Mark III data set.



Eq. 7 is strictly applicable only in the case of a single attractor, as peculiar velocities can be added under the hypothesis, valid in linear theory (and even beyond, see Susperregi & Buchert, 1997) that they are proportional to peculiar acceleration. However, eq. 7 reduces to linear theory almost anywhere, except in the proximity of an attractor, where the contributions from all the other attractors are weak. Therefore, the non-linear formula is considered as a suitable approximation for the velocity field generated by the attractors. As a consistency check, we have verified that the use of pure linear theory does not change significantly the obtained values of the free parameters, with the exception of  $\Omega_0$ , which can not be disentangled from the normalization mass factor  $A$  of eq. 4 if no non-linearity is taken into account.

Specifically, we assume that the perturbing masses are: 1) the Virgo cluster (V), which gives rise to distortions in the Hubble flow of LG surrounding regions (e.g., de Vaucouleurs & Boldingher, 1979; Tonry & Davis, 1981); 2) the Great Attractor (GA), which seems the best candidate to explain large scale galaxy motions inside a volume of radius 5000-10000 km s<sup>-1</sup> (Burstein et al., 1986; Dressler et al., 1987); 3) Perseus-Pisces (PP), a large and irregular supercluster, whose massive filamentary structure seems to be concentrated at a redshift of about 5000 km s<sup>-1</sup> in the antipodal direction of GA (Willick 1991; Han & Mould 1992; Courteau et al., 1993); 4) the Shapley concentration (SH), a very rich concentration of  $\sim 25$  galaxy clusters whose mean complex lies at 14000 km s<sup>-1</sup> and is located behind the GA region (Scaramella et al., 1989). SH stands out as the richest optical supercluster of the entire sky within  $z < 0.1$  (Zucca et al., 1993).

In our final analysis we do not consider the possible gravitational influence of the Coma Supercluster, because we have checked that its inclusion does not improve the goodness of the fit (see, e.g., Shaya, Tully & Pierce, 1992, who reached the same conclusion in their less sensitive analysis of a galaxy sample limited to  $cz = 3000$  km s<sup>-1</sup>).

In the fit we do not consider the few very nearby galaxies having  $cz < 700$  km s<sup>-1</sup> and we do not correct their tabulated distances. These galaxies are believed to share with the LG a bulk motion (the so-called Local Anomaly) perpendicular to the supergalactic plane (Faber & Burstein, 1988). The Local Anomaly is a perturbation term introduced in the standard picture of the peculiar velocity field of the very nearby universe in order to explain the discrepancy between the observed and the predicted radial velocities of the LG with respect to the CMB. It is in general interpreted as a due to the "negative gravity" of the "Local Void" (Tully & Fisher, 1987) which is located above the supergalactic plane.

After we have specified for each galaxy the redshift  $cz_i$  and the distance  $r_i$ , the  $\chi^2$  expression (see eq. 6) becomes a known function of several parameters. The free parameters which describe mass distribution and geometry are, for each attractor,  $A_i$ ,  $r_{ci}$ . Furthermore, in the case of GA and SH, we have decided to leave free the Galactic coordinates  $l$ ,  $b$  of their centers and also the distance of GA from

us. Finally, we try to leave  $\Omega_0$  as a further free parameter. We take, instead, from the literature the values for the positions of PP ( $l = 120^\circ$ ,  $b = -30^\circ$ ,  $r = 5000$  km s<sup>-1</sup>) and V ( $l = 284^\circ$ ,  $b = 74^\circ$ ,  $r = 1350$  km s<sup>-1</sup>), and the distance of SH ( $r = 14000$  km s<sup>-1</sup>).

Thus, we are left with 13 degrees of freedom. Solutions may be unstable or physically not meaningful in the presence of so many parameters. However our data set is very large and quite uniform in spatial distribution so much to prevent statistical artifacts. Moreover, the improved accuracy in estimated distances ensures confidence in the possibility of constraining different models through the minimization procedure. Lastly, if we assume that the significance of each parameter is related to the change in likelihood of the best fit that results from its addition to the model, our trials with models having less parameters confirm the validity of the best fits achieved with many degrees of freedom. Nevertheless, the  $\chi^2$  minimization scheme may introduce biased results due to the incompleteness of the dataset. For example, the redshift limit of Mark III catalog, which does not map distant regions of the universe, could constrain in a wrong way the parameters of the Shapley concentration.

The  $\chi^2$  significance is ill-defined because velocity errors are coupled and because it depends considerably on the size of the distance errors and velocity spread due to noise in the velocity field. Encouragingly, we have checked that different values of the velocity spread (taken as constant in space) have little influence on the attractor parameters. In any case, we do not use the  $\chi^2$  statistics to assess the validity of a model. We are interested in the relative decrease of the  $\chi^2$  values, because the purpose of our analysis is to obtain a redshift-distance relation having less scatter and systematic bias than that of the simple unperturbed Hubble flow.

### 3.2.2 Model-fitting results

Using various subsamples we estimate the attractor parameters separately in order to examine their reliability and stability.

In Tables 2 and 3 we present the data number  $N$ , the values of  $\chi^2/dof$  and *rms* dispersions of model velocity residuals  $\sigma(cz)$  (in km s<sup>-1</sup>) relative to Mark II and Mark III data for Hubble flows in the CMB frame and in the LG frame, respectively.

We report results for the whole Mark II and for a Mark II subsample (Mark II\*) which does not include the spirals by de Vaucouleurs & Peters (1984) and the field ellipticals. The omission of the former subsample is motivated by the fact that it does not appear in the subsequent compilation (Mark III). The omission of the latter is justified by the fact that many ellipticals reside in systems of fairly high velocity dispersion and hence, can not be retained as good tracers of the velocity field. In these tables we give also the results relative to the various Mark III subsamples (denoted as described in §2), to the Mark III spirals (Mark III\*) and the entire Mark III.

In Table 4 we give the minimization results (together

Fig. 3.— The plots show the radial components (in the CMB frame) of the velocity fields in the supergalactic plane  $SGX, SGY$  for the multi-attractor model fitted to the Mark II subsample (left) and the whole Mark III (right). The arrows and the boldface arrows distinguish between incoming and outgoing objects. The contours correspond to the same radial peculiar velocity; contour spacing is  $100 \text{ km s}^{-1}$ , with the heavy contour marking 0. Regions of different radial peculiar velocities are also indicated by shading. The Local Group is at the center, the Great Attractor is on the left, and Perseus-Pisces is on bottom right. Coordinates are expressed in  $\text{km s}^{-1}$ .

Fig. 4.— The plots show the velocity field in the CMB frame for the multi-attractor model fitted to the Mark II subsample (left) and the whole Mark III (right). The vectors shown are projections of the 3D velocity field in the supergalactic plane  $SGX, SGY$ . The contours correspond to the same velocity vector modulus; contour spacing is  $100 \text{ km s}^{-1}$ , with the heavy contours marking  $200 \text{ km s}^{-1}$  and  $300 \text{ km s}^{-1}$  for the Mark II subsample and the Mark III, respectively. Regions of different peculiar velocities are also indicated by shading. The Local Group is at the center and the Great Attractor is on the left. Coordinates are expressed in  $\text{km s}^{-1}$ .

TABLE 2

THE HUBBLE FLOW MODEL IN THE CMB FRAME.

	Mark II*	Mark II	A82	MAT	HMCL	WCF	E/SO	Mark III*	Mark III
$\mathcal{N}$	413	662	192	277	36	65	250	570	820
$\chi^2/dof$	1.90	1.70	1.43	1.16	1.97	1.30	3.00	1.22	1.97
$\sigma(cz)$	698	835	1020	634	696	851	977	812	873

TABLE 3

THE HUBBLE FLOW MODEL IN THE LOCAL GROUP FRAME.

	Mark II*	Mark II	A82	MAT	HMCL	WCF	E/SO	Mark III*	Mark III
$\mathcal{N}$	413	662	192	277	36	65	250	570	820
$\chi^2/dof$	2.10	1.71	1.22	1.49	1.96	1.34	3.24	1.41	1.97
$\sigma(cz)$	682	790	943	661	627	1032	955	804	858

TABLE 4

THE BEST-FITTING PARAMETERS FOR THE MULTI-ATTRACTOR MODEL.

	Mark II*	Mark II	A82	MAT	HMCL	WCF	E/SO	Mark III*	Mark III
$\mathcal{N}$	413	662	192	277	36	65	250	570	820
$\chi^2/dof$	0.94	0.99	0.69	1.08	0.97	0.78	2.60	0.98	1.48
$\sigma(cz)$	543	686	757	618	415	739	903	713	787
$A_V$	3.1±0.6	2.9±0.8	4.5±0.8	0	0	0	2.0±1.2	4.0±0.95	3.1±1.6
$A_{GA}$	2.9±0.5	3.0±0.7	3.7±0.9	0	3.2±1.0	3.9±1.4	3.5±0.7	1.5±0.5	2.4±1.0
$A_{PP}$	1.0±0.7	-	3.2±1.7	0	4.0±1.2	2.8±1.0	0	3.4±0.7	2.6±1.1
$A_{SH}$	1.0±0.9	-	0	5.0±2.0	4.2±1.2	0	2.0±0.9	4.6±1.4	3.3±1.4
$r_{c,V}$	530±30	500±30	500±28	0	0	0	490±44	480±73	498±30
$r_{c,GA}$	2080±45	1740±70	1950±82	0	1830±70	1930±110	2500±68	1820±112	1806±70
$r_{c,PP}$	1480±150	-	1440±110	0	900±50	2200±110	0	1410±60	1415±61
$r_{c,SH}$	2450±170	-	0	2500±130	3000±50	0	2725±80	2930±50	3004±35
$l_{GA}$	305°±4°	309°±4°	294°±6.5°	-	314°±3°	303°±3°	309°±3°	300°±18°	309°±5°
$b_{GA}$	15°±3°	18°±3°	17°±4°	-	0°±6°	5°±3°	10°±3°	25°±19°	18°±3°
$d_{GA}$	4170±40	4170±50	4150±30	-	4200±90	4200±40	4400±110	4200±105	4200±30
$l_{SH}$	312°±9°	-	-	319°±3°	319°±6°	-	308°±4°	308°±10°	308°±5°
$b_{SH}$	27°±5°	-	-	8°±5°	3°±4°	-	2°±5°	2°±13°	4°±5°
$\Omega_0$	0.8±0.2	1.0±0.2	0.6±0.3	0.5±0.3	0.5±0.2	0.8±0.3	0.2±0.2	0.6±0.2	0.4±0.3

with  $1\sigma$  errors) relative to Mark II and Mark III for our multi-attractor model; the values of the GA distance  $d_{GA}$ , attractor radii  $r_c$ , and model velocity residuals  $\sigma(cz)$  are given in  $\text{km s}^{-1}$ . We have checked that the inclusion of PP and SH did not improve significantly the fit to the whole Mark II, so that only two attractors (Virgo and GA) are adopted in this case.

For some parameters, in Fig. 5 we show the ellipses of confidence (at the 68% and 90% significance levels) obtained from the covariance matrix, according to the model fitted to the whole Mark III. Fig. 3 shows the radial velocity fields (in the supergalactic plane  $SGX, SGY$ ) of the

multi-attractor models relative to the Mark II subsample and the whole Mark III. Fig. 4 show the respective velocity fields.

From an inspection of Tables 2, 3, and 4 we can draw the following comments. Velocity field models improve the fit with respect to the unperturbed Hubble flow in a decisive way, and a multi-attractor model is the best way to trace out the underlying observed velocity field. Only for the MAT sample, a bulk motion generated by SH seems to be best solution. On the other hand, the fact that the uniform expansion model in the LG frame generally fits the data much better than that in the CMB frame strengthens

the evidence for a large streaming motion occurring along the PP-GA baseline and flowing towards SH.

We stress that for most Mark III samples the best fit is obtained if SH is included in the velocity field models. Only in A82 and WCF subsamples the long range action of this supercluster is undetected, probably because the former sample maps only the LS dynamics and the latter mostly covers the region surrounding PP, which introduces incompleteness biases in the  $\chi^2$  statistics.

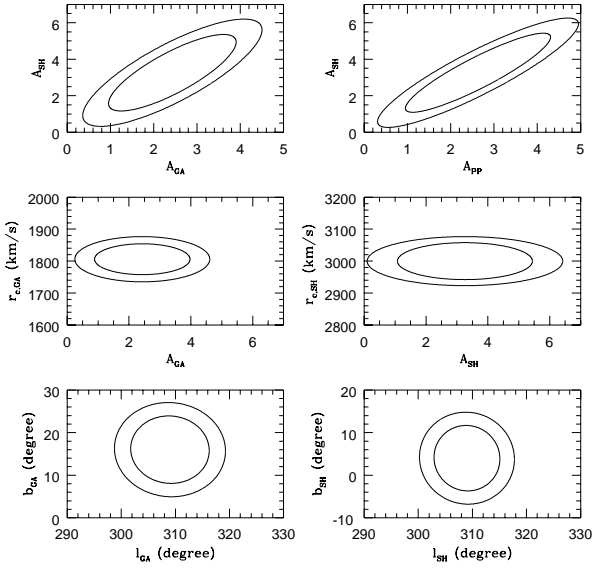


Fig. 5.— For some parameters, we show the regions of confidence (at the 68% and 90% significance levels) according to the model fitted to the whole Mark III.

In every subsample the application of velocity corrections reduces considerably both scatter and  $\chi^2$ .

The reduction in scatter is more evident in the A82, HMCL, WCF subsamples which have more accurate distance estimates (see the relative  $\sigma$ -values in Tables 2, 3, and 4). Figs. 6, 7, and 8 show the recession velocity (in the CMB frame) versus the distance before and after correction for peculiar motions as predicted by models fitted to the three aforementioned subsamples. These figures clearly illustrate how closer to the Hubble line our corrected data lie than original data do.

An independent way to judge the validity of a model is to look at the velocity deviations from model predictions as a function of the distance. Fig. 9 shows that, for the attractor models of the Mark II subsample and whole Mark III, the residuals (*observed* minus *calculated* velocity) exhibit no overall systematic variation with distance, as is expected for a good model.

The position of the GA obtained from various Mark III subsamples is almost similar and stable. The whole Mark II and Mark III yield  $l = 309^\circ$   $b = 18^\circ$  for the GA as in Faber & Burstein (1988). Our best fit of the whole Mark III locates the mass center of SH at  $l = 308^\circ$   $b = 2^\circ$ , which somewhat differs from the position of the optical

center ( $l = 319^\circ$ ,  $b = 27^\circ$ ) as reported by Scaramella et al. (1989). Interestingly, all Mark III subsamples tend to locate SH at low  $b$ -values with respect to the optical position; this suggests that there is more matter behind the Galactic plane than previously thought. Ongoing redshift surveys in the SH region (e.g., Proust, Quintana & Slezak, 1998) will be able to investigate on the possible SH extension towards the zone of avoidance.

The relative values of the radii  $r_c$  give some insight into the distribution of matter inside the attractors. The large  $r_c$ -values of GA and SH indicate that they are not peaks of highly clumped matter, but rather large overdensity regions. In particular, the GA mass is substantially distributed across a distance of  $\sim 2000$  km s $^{-1}$  (Faber & Burstein (1988) quoted the value of 1500 km s $^{-1}$  for a different model); the PP core radius is  $\sim 1400$  km s $^{-1}$ ; the SH core radius is  $\sim 3000$  km s $^{-1}$ , whereas the optical radius, defined as the radius of a sphere centered in SH and containing  $\sim 25$  (or  $\sim 15$ ) rich clusters, is  $\sim 5000$  km s $^{-1}$  (or  $\sim 1500$  km s $^{-1}$ ) (Vettolani et al., 1990; Bardelli et al., 1994).

The normalizing mass parameters  $A_i$ , which are left as free parameters, bear no immediate interpretation. However, these values are used to evaluate interesting physical quantities, such as the masses of the attractors or the infall velocities that they generate.

To estimate the excess mass in the attractor regions, we evaluate the volume integral of the mass distribution we adopted (the King profile of eq. (4)). This is a crude approximation because of the possible strong departure of the mass distribution from spherical symmetry; we suppose that anisotropies in the density field cancel out when averages over a large volume of space. For a sphere centered in GA and having LG on its border, the whole Mark II yields a mass of  $(5.1 \pm 2.5) \cdot 10^{16} \cdot h^{-1} M_\odot$ , whereas Lyndell-Bell et al. (1988), using only the elliptical sample, reported the value of  $5.4 \cdot 10^{16} M_\odot$ , and Shaya et al. (1992) reported  $1.5 \cdot \Omega_0^{0.4} \cdot 10^{16} M_\odot$ . The whole Mark III gives a smaller mass of  $(1.8 \pm 1.6) \cdot 10^{16} h^{-1} M_\odot$ .

If we consider the attractors as spheres of radius  $r_c$ , we obtain the excess masses reported in Table 5 for our multi-attractor models fitted to some data subsets (Mark II subset, Mark III spirals, whole Mark III). Table 5 lists also the density contrast averaged over a sphere centered on the attractor and having the LG on its border.

According to Mark III and Mark II, Virgo is confirmed to be a poor cluster; it has an excess mass of  $1.3 \cdot 10^{14} h^{-1} M_\odot$  (see Table 5) and a total mass of  $2.0 \cdot 10^{14} h^{-1} M_\odot$  according to Mark III data ( $2.2 \cdot 10^{14} h^{-1} M_\odot$  and  $3.2 \cdot 10^{14} h^{-1} M_\odot$  according to Mark III spiral data, respectively). These values are substantial agreement with the estimates of masses based on optical and X-ray data. From optical data Girardi et al. (1998) estimated a virial mass of  $M = (2.7_{-0.4}^{+0.5}) 10^{14} h^{-1} M_\odot$  within a virialization radius of  $1.69 h^{-1}$  Mpc. From ROSAT PSPC X-ray observations Nulsen & Böhringer (1995) estimated a cluster mass per unit length of  $1.24 \cdot 10^{11} M_\odot kpc^{-1}$ , which is

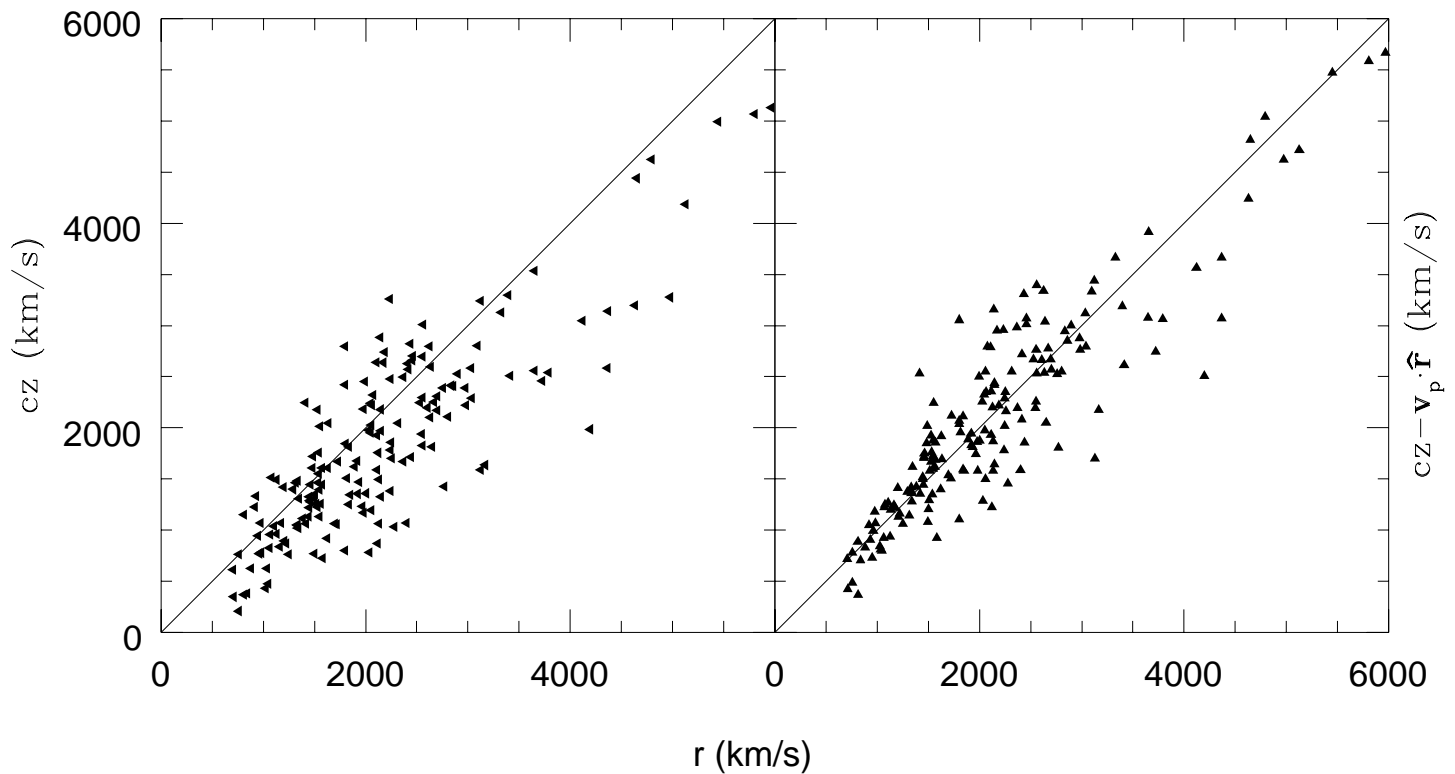


Fig. 6.— These plots show the recession velocity  $cz$  (in the CMB frame) as a function of the distance  $r$  (in km/s) before (left) and after (right) corrections for peculiar motions, as predicted by the multi-attractor models fitted to the A82 galaxy sample. The scatter decreases from  $\sigma = 1020$  (left)  $\text{km s}^{-1}$  to  $\sigma = 757$   $\text{km s}^{-1}$  (right).

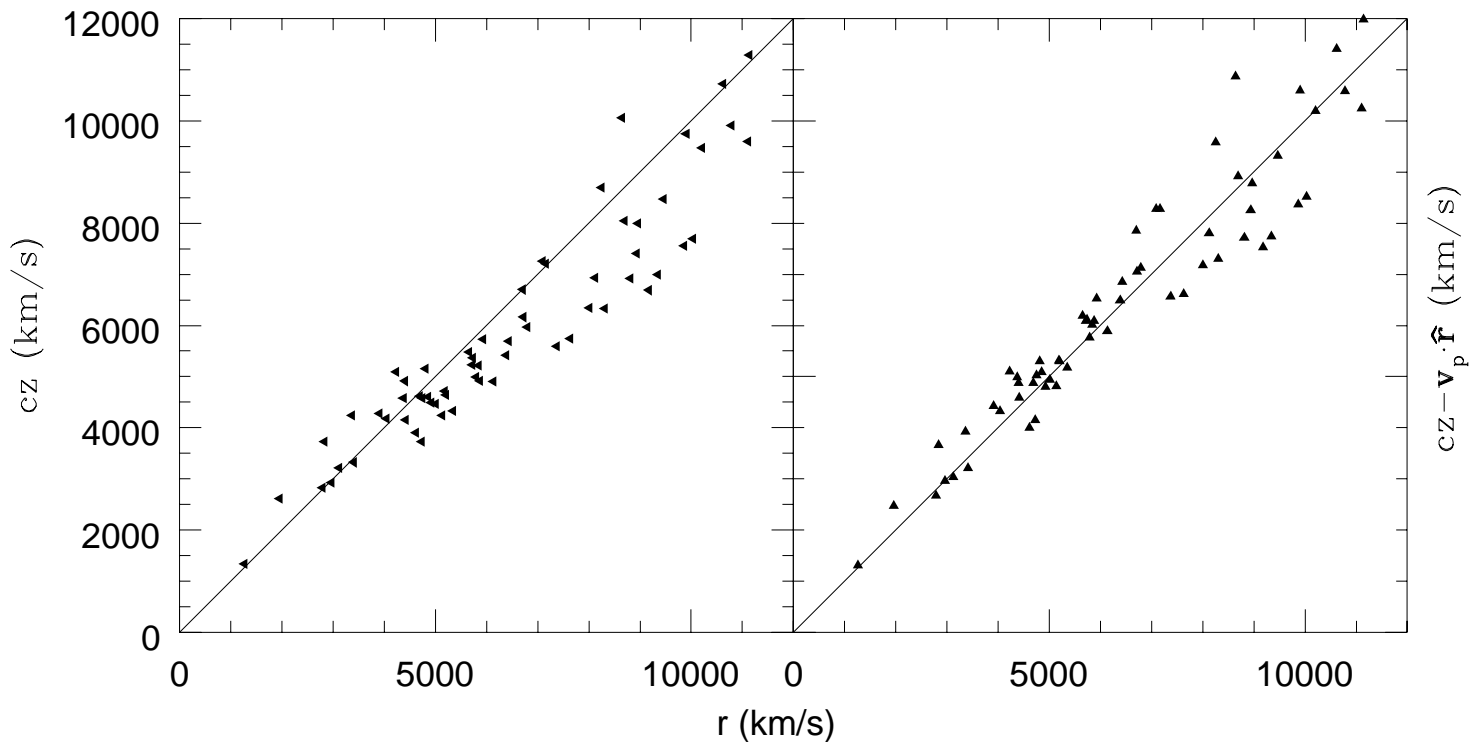


Fig. 7.— The same as in Fig. 6 for the multi-attractor model fitted to the WCF sample. The scatter decreases from  $\sigma = 851$   $\text{km s}^{-1}$  (left) to  $\sigma = 739$   $\text{km s}^{-1}$  (right).

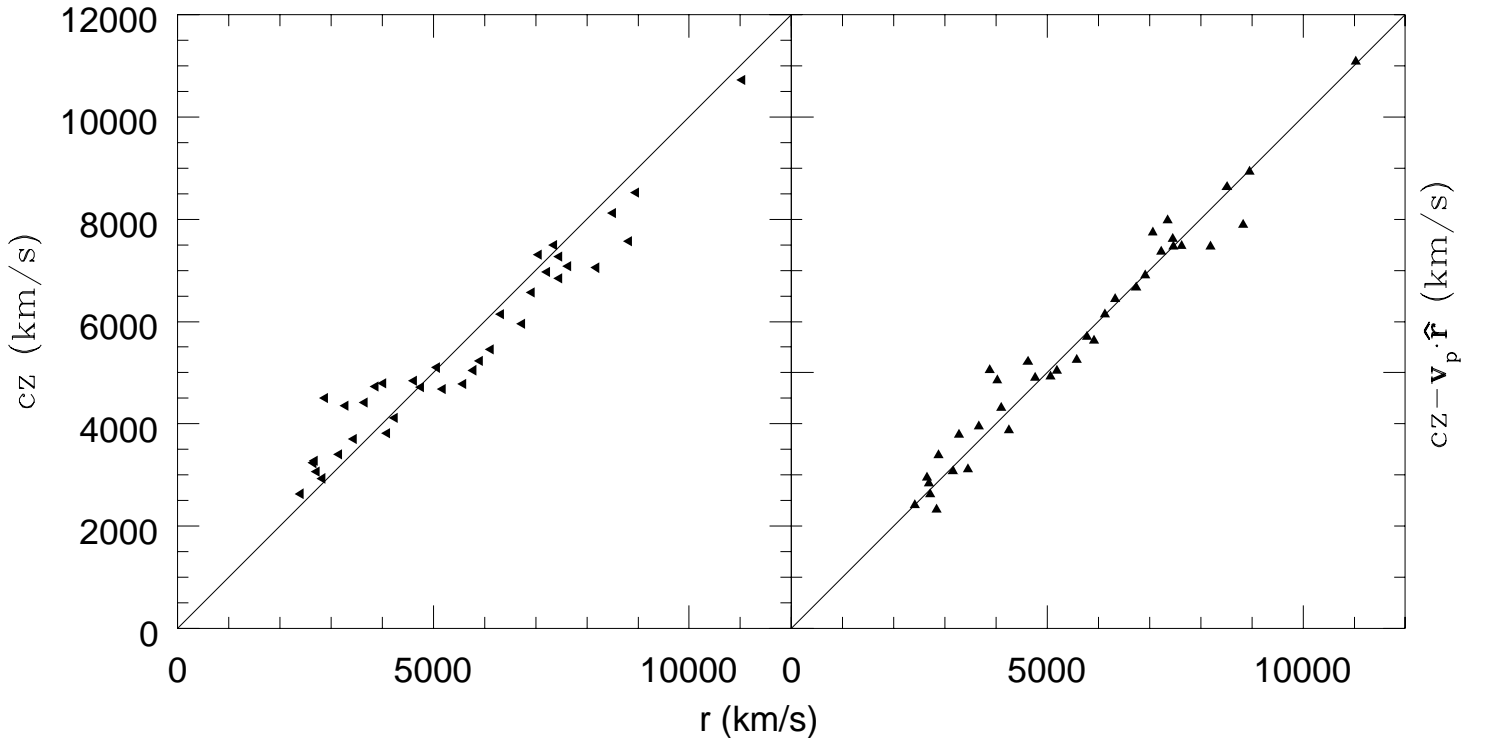


Fig. 8.— The same as in Fig. 6 for the multi-attractor model fitted to the HMCL sample. The scatter decreases from  $\sigma = 696$   $\text{km s}^{-1}$  (left) to  $\sigma = 415$   $\text{km s}^{-1}$  (right).

consistent with our estimates, if we use an isothermal sphere extrapolation ( $M(r) \propto r$ ).

Compared to Mark II, Mark III data stress the role of PP and SH (see also the  $A_i$ -values listed in Table 4), whilst they give a less prominent GA with a mass which is roughly comparable to the PP mass and is  $\sim 5$  times smaller than the SH mass. This is in good agreement with Scaramella et al.'s (1989) finding that in optical maps the SH region contains 5 times as many rich clusters as the GA region does. The SH excess mass derived from Mark III ( $3 - 5.7 \cdot 10^{16} h^{-1} M_\odot$ , see Table 5) (as well as the corresponding SH total mass of  $4.7 - 8.1 \cdot h^{-1} \cdot 10^{16} M_\odot$ ) is roughly consistent with values intermediate between upper and lower limits based on optical and X-ray data. From the velocity dispersion of the SH clusters Raychaudhury et al. (1991) and Quintana et al. (1995) obtained

upper limits to the total mass of  $1.3 \cdot 10^{17} h^{-1} M_\odot$  and  $7 \cdot 10^{16} h^{-1} M_\odot$ , respectively.

Assigning to the 40 SH clusters the virial mass of  $3 \cdot 10^{14} h^{-1} M_\odot$ , which is the average of the virial masses deduced for 10 SH clusters, Quintana et al. (1995) estimated a lower limit for the SH mass of  $1.2 \cdot 10^{16} h^{-1} M_\odot$ . From the X-ray luminosities of the 12 brightest clusters, scaling to the Coma cluster (with  $L_X \propto M^{0.4}$ ), Raychaudhury et al. (1991) obtained a lower limit of  $9 \cdot 10^{15} h^{-1} M_\odot$ . From the analysis of the ROSAT PSPC and *Einstein Observatory* IPC X-ray observations Ettori, Fabian & White (1997) derived a lower limit for the dynamical SH mass of  $6 \cdot 10^{15} h^{-1} M_\odot$ ; their virial mass estimate is  $\sim 5$  times larger than the last value. From the SH influence on local flows Shaya et al. (1992) reported a large dynamical mass of  $2.6 \cdot \Omega_0^{0.4} 10^{17} M_\odot$ . The same authors obtained a PP

TABLE 5

THE EXCESS MASSES AND DENSITY CONTRASTS FOR THE ATTRACTORS.

Attractors	Mark III		Mark III(spirals)		Mark II(subset)	
	$M(< r_c)$ ( $M_\odot h^{-1}$ )	$\langle \delta_0 \rangle_{LG}$	$M(< r_c)$ ( $M_\odot h^{-1}$ )	$\langle \delta_0 \rangle_{LG}$	$M(< r_c)$ ( $M_\odot h^{-1}$ )	$\langle \delta_0 \rangle_{LG}$
Virgo	$(1.3 \pm 1.3) \cdot 10^{14}$	$0.36 \pm 0.22$	$(2.2 \pm 1.5) \cdot 10^{14}$	$0.44 \pm 0.23$	$(2.8 \pm 1.5) \cdot 10^{14}$	$0.35 \pm 0.30$
GA	$(4.7 \pm 4.4) \cdot 10^{15}$	$0.38 \pm 0.18$	$(4.4 \pm 3.0) \cdot 10^{15}$	$0.24 \pm 0.11$	$(1.6 \pm 0.6) \cdot 10^{16}$	$0.44 \pm 0.10$
PP	$(2.4 \pm 2.2) \cdot 10^{15}$	$0.19 \pm 0.09$	$(4.7 \pm 2.7) \cdot 10^{15}$	$0.23 \pm 0.06$	$(1.5 \pm 2.1) \cdot 10^{15}$	$0.07 \pm 0.07$
Shapley	$(3.0 \pm 2.7) \cdot 10^{16}$	$0.12 \pm 0.05$	$(5.7 \pm 3.7) \cdot 10^{16}$	$0.16 \pm 0.06$	$(8.0 \pm 9.8) \cdot 10^{15}$	$0.02 \pm 0.02$

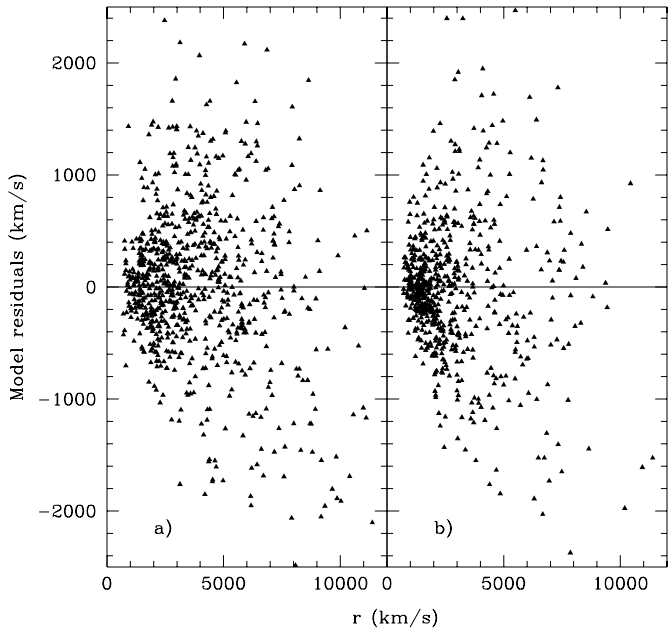


Fig. 9.— We show the residual (*observed minus calculated*) velocities versus the distance  $r$  (in  $\text{km s}^{-1}$ ), for the velocity models fitted to the whole Mark III (a) and the Mark II subsample (b).

dynamical mass of  $5 \cdot \Omega_0^{0.4} 10^{16} M_\odot$ , which better agrees with our estimates than their SH mass does. The best-fitting values of  $\Omega_0$  tabulated in Table 4 are used for the estimates given above.

We have also computed the infall velocity generated by Virgo alone at the LG position. We find  $v = 170 \pm 64 \text{ km s}^{-1}$ ,  $v = 145 \pm 57 \text{ km s}^{-1}$ , and  $v = 96 \pm 45 \text{ km s}^{-1}$  for the A82 sample, the Mark III spiral sample, and the whole Mark III, respectively. In particular the last low value indicates that Virgo infall is not a major source of the velocity field in the LS, in agreement with several recent results and in disagreement with the results of the modified cluster dipole model (see end of §3.1.2).

Remarkably, the influence of the GA at the LG position is lower than expected from Mark II and from previous results.

TABLE 6

THE MOTION OF THE LOCAL GROUP IN THE CMB FRAME.

Sample	l	b	$\theta$	V	$V_{\parallel}$
Mark II(subset)	305°	25°	25°	705	567
Mark II	307°	29°	26°	666	563
A82	290°	30°	11°	479	615
MAT	310°	7°	48°	412	491
HMCL	318°	0°	49°	810	410
WCF	310°	0°	43°	225	456
E/SO	309°	12°	34°	556	516
Mark III(spirals)	309°	7°	37°	454	496
Mark III	309°	12°	36°	488	511

The pull generated by GA at the LG position turns out to be  $v = 314 \pm 200 \text{ km s}^{-1}$  according to Mark III data (it is  $v = 620 \pm 260$  according to Mark II data). Therefore, nearly one half of the LG motion is due to the SH action. At variance with Mark II, Mark III data suggest that the SH, projected behind the GA, yields a pull on the LG comparable to that exerted by GA.

There is a way to test the relative prominence of the GA without resorting to any specific attractor modeling. It suffices to assume that the infall on the attractor be radial and that we know fairly well its angular position in the sky. Let us take a sphere centered at half the distance between LG and GA, with LG on its border. Now if the infall is radial and GA is the only responsible for the observed flow patterns, then, for a simple geometrical reason, the galaxies lying inside the sphere should have positive peculiar velocities, whilst the galaxies lying outside should have negative radial components (see Fig. 10); only at the surface of the sphere the radial components would become null.

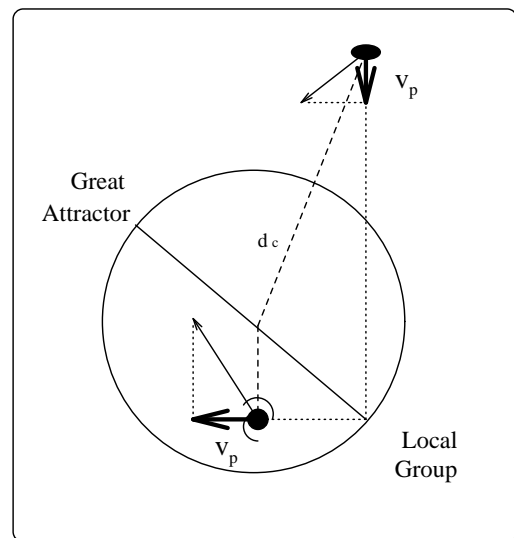


Fig. 10.— The plot illustrates the following concept: for a sphere centered at half the distance between the Local Group and the Great Attractor, under the hypothesis of a radial infall on the Great Attractor only, a galaxy which is at distance  $d_c$  from the center of the sphere and lies inside (outside) the sphere should have a positive (negative) radial peculiar velocity  $v_p$  (as viewed from an observer placed in the Local Group).

In Fig. 11 we compare the results obtained with Mark II and Mark III data. Mark II and A82 data (see Fig. 11d, f, respectively) favour a massive GA dominating large scale motions, whilst evidence for this is considerably weakened in other Mark III samples, which do not show a clear radial infall pattern towards GA. This can be only partially due to the perturbing presence of PP, because if we exclude the galaxies located in the PP region from the plot (see

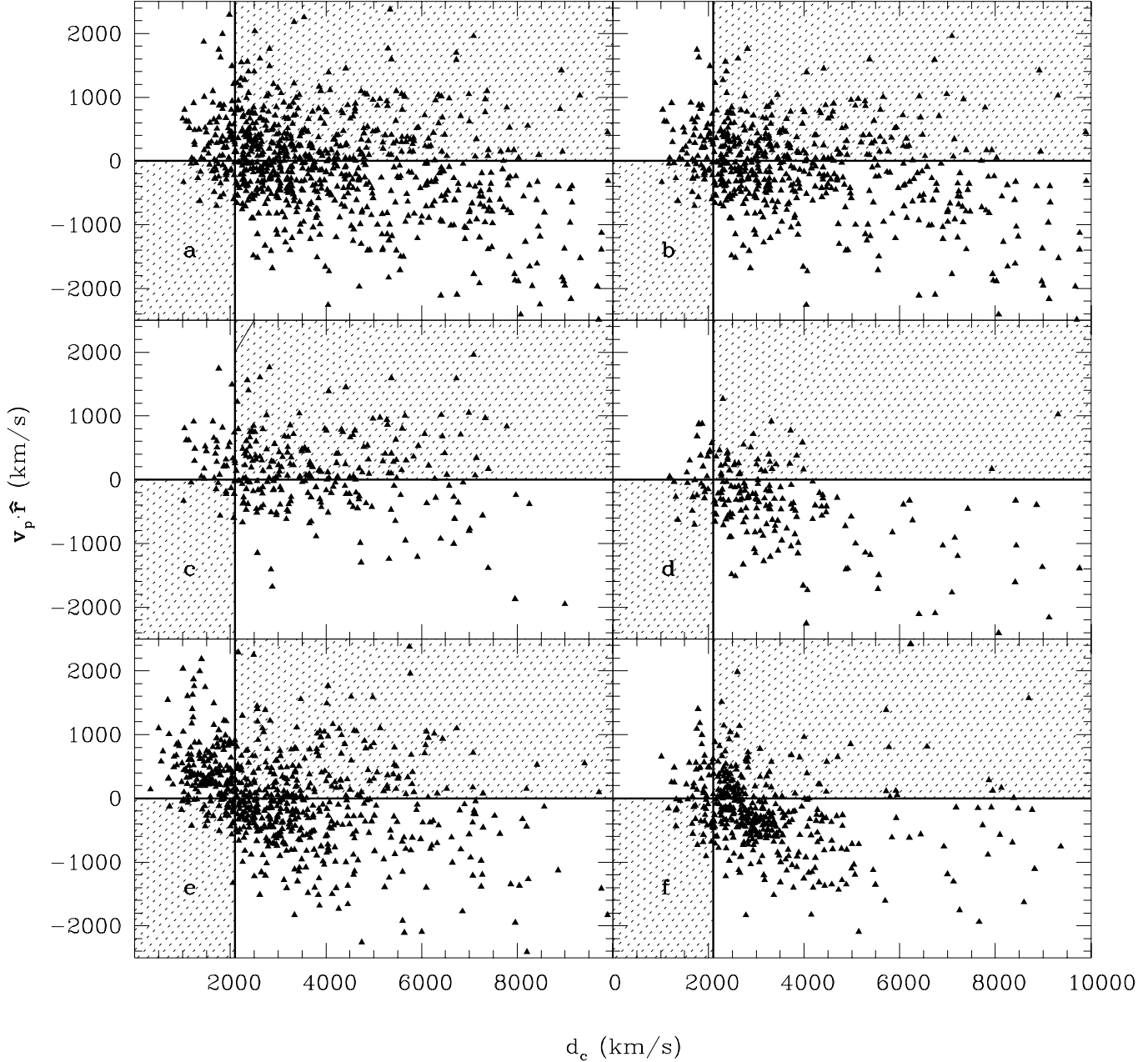


Fig. 11.— The observed radial peculiar velocities  $v_p$  (in  $\text{km s}^{-1}$ ) as a function of the distance  $d_c$  (in  $\text{km s}^{-1}$ ) from the middle point of a line joining the Great Attractor with the Local Group. If the Great Attractor were the only source of radial infall, then for  $d_c > 2100 \text{ km s}^{-1}$  peculiar velocities should be negative, while for  $d_c < 2100 \text{ km s}^{-1}$  they should be positive (see Fig. 10). We consider various samples of galaxies: the whole Mark III data (a), the Mark III spirals (b) (almost all Mark III ellipticals lie in the GA region), the MAT 82 spirals (c), the A82 spirals (d), the Mark III sample without the objects located in the Perseus-Pisces region (i.e., those placed inside a sphere centered on this supercluster and having a radius of  $3000 \text{ km s}^{-1}$ ) (e), the whole Mark II data (f).

Fig. 11e), there are still many galaxies with positive peculiar velocity components.

This reflects the lack of a back-side infall towards GA or, in other words, the long range effect of SH which prevents galaxies located in the back of GA to acquire negative pe-

culiar velocity components.

If the GA were the dominant system we would expect a GA back-infall to be comparable in amplitude to the GA forward-infall. On the contrary, if SH exerts a significant gravitational influence, we expect an asymmetry in



the amplitudes of the back- and forward-infalls, i.e. positive components outside the sphere. In conclusion, local samples such as the A82 sample and Mark II, which does not include many galaxies in the back of GA, can not fully reveal the importance of SH in determining peculiar motions.

In Fig. 12 we show the mean overdensity profile inside a spherical volume centered on each attractor, for our model of the whole Mark III. The PP and GA overdensities at  $r \sim 1200 \text{ km s}^{-1}$  are in reasonable agreement (being just a bit higher) with the density peaks at  $1200 \text{ km s}^{-1}$  Gaussian smoothing, ( $\delta_0 \sim 1.2$  and  $\sim 1.4$ , respectively) found by Sigad et al. (1998) who used the POTENT procedure to reconstruct the smoothed mass density field from Mark III data (for  $\Omega_0=1$ ), taking into account mild non-linear effects. These mass density peaks are not much different from the reconstructed real-space density peaks (at  $1200 \text{ km s}^{-1}$  Gaussian smoothing) of IRAS galaxies ( $\delta_0 \sim 0.8$ ; see Sigad et al., 1998) and optical galaxies ( $\delta_0 \sim 1.8$  and  $0.8$ , respectively; see Hudson et al., 1995), which is in line with the widespread contention that mass and galaxies are related via an approximate linear biasing relation with a biasing factor  $b_c$  of order unity.

In Table 6 we report the direction  $(l, b)$  and the amplitude  $V$  of the CMB anisotropy dipole generated by the assumed distribution of attracting masses, for multi-attractor models relative to various subsamples. We also give the angular separation  $\theta$  between the observed and reconstructed dipole together with the projection  $V_{\parallel}$  of the observed CMB dipole in the  $(l, b)$  direction. In all cases the reconstructed dipole shows a satisfactory agreement both in direction and in amplitude with the observed dipole.

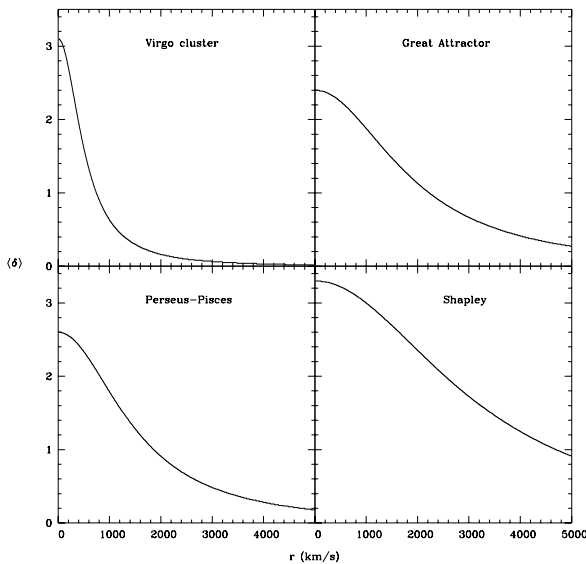


Fig. 12.— The plots show the density contrast, averaged over spheres centered on each attractor, as a function of the distance  $r$  (in  $\text{km s}^{-1}$ ) from the attractor, for the velocity model fitted to the whole Mark III data.

This can be taken as an independent evidence of the reliability of the multi-attractor toy model we used.

The remaining differences between the observed and reconstructed dipole can be justified in several ways. For example, inhomogeneities beyond  $15000 \text{ km s}^{-1}$  could contribute significantly to the LG motion (e.g., Branchini, Plionis & Sciama, 1996; Plionis & Kolokotronis, 1998) or, according to an alternative explanation, the motions of the very nearby galaxies are also subjected to the Local Anomaly (Burstein, 1990). If we preferred the latter explanation, we would reconstruct a Local Anomaly velocity vector with an amplitude of  $370 \text{ km s}^{-1}$  pointing in the direction  $l = 212^\circ$ ,  $b = 35^\circ$ , which is not much different from that reported by Faber & Burstein (1988) ( $v = 360 \text{ km s}^{-1}$ ,  $l = 199^\circ$ ,  $b = 0^\circ$ ) and is greater in amplitude than that obtained by Han & Mould (1990) ( $v = 240 \text{ km s}^{-1}$ ,  $l = 205^\circ$ ,  $b = 11^\circ$ ).

In our minimizing scheme Mark II data favour  $\Omega_0$ -values close to 1, whereas Mark III subsamples tend to give lower  $\Omega_0$ -values (the whole Mark III and the Mark III spirals give  $\Omega_0 = 0.4 \pm 0.3$  and  $\Omega_0 = 0.6 \pm 0.2$ , respectively). Although the exact estimate of  $\Omega_0$  may be seriously affected by our specific modeling of the density field in which the detailed features of density fluctuations are neglected, the tendency towards lower  $\Omega_0$ -values is meaningful and agrees qualitatively with the coming down of the estimates of the parameter  $\beta$  resulting from the comparison between the (Mark II and Mark III) observed velocity field and that predicted by the IRAS galaxy densities ( $\beta \sim 0.4$ – $0.9$ , with the lowest values favored by the most recent works; see, e.g., Sigad et al., 1998). Notably, a comparison between the IRAS galaxy density fields and the mass density fields reconstructed from the application of the POTENT method to Mark II (Dekel et al., 1993) and Mark III (Sigad et al., 1998) data shows a similar tendency, with systematically greater values of  $\beta$  ( $\beta \sim 1.3$  and  $\sim 0.9$ , as reported in the respective papers). Reasons for the systematic differences in  $\beta$ -values obtained from comparing fields at density and velocity levels have been discussed by Willick et al. (1997b) and Willick & Strauss (1998). Direct comparison of densities is a local procedure, whereas comparison of velocities is non-local, because the velocity field is sensitive to the mass distribution in a large volume, even outside the sampled volume (e.g., the Shapley concentration). This non-local character is also inherent to our approach and may cause our results to better agree with those resulting from velocity–velocity comparisons.

Also very recent papers, which followed this kind of approach, favored fairly low values of  $\beta$ , by using new samples of velocity field tracers. Da Costa et al. (1998) found  $\beta \sim 0.6$  from an extensive I-band TF sample of spiral galaxies, the SFI catalog (e.g., da Costa et al., 1996). Riess et al. (1997) obtained  $\beta \sim 0.4$  from a sample of Type Ia supernovae.

In conclusion, our best estimate of  $\Omega_0$  converges towards the (inelegant) value of  $\sim 0.5$ , which roughly corresponds to the average of many estimates of  $\Omega_0$  resulting from the

analyses of large scale structure and cosmic flows. Studies based on non-linear dynamics within galaxies, groups, and clusters (on scales of  $\sim 1 - 10 h^{-1}$  Mpc) yield low values of  $\Omega_0 \sim 0.2-0.3$  (see the review by Dekel, Burstein & White, 1997).

#### 4 INVERTING THE REDSHIFT-DISTANCE RELATION: THE TRIPLE-VALUED REGIONS.

We use three basic models derived in the previous section, i.e. the modified cluster dipole model and the four-attractor models relative to the Mark II subset and the Mark III spirals, for providing numerical and explicit expressions of the recession velocity  $cz$  (expressed in the LG frame) as a non-linear function of distance  $r$ . In general, this relation, coupled with the heliocentric redshift tabulated in Garcia et al. (1993) and transformed by us in the LG frame according to the relation  $cz_{LG} = cz_{\odot} - 79 \cos l \cos b + 296 \sin l \cos b - 36 \sin b$  (with  $cz$  in  $\text{km s}^{-1}$ ) (Yahil, Sandage & Tamman, 1977), gives the galaxy distance. The galaxy groups are given the median values of the coordinates and redshifts of the group members, selected according to the final catalog by Garcia (1993). As already said in §3.2.1, because of the Local Anomaly problem, for the four-attractor model we do not invert the redshift-distance relation for the few very nearby galaxies ( $cz < 700 \text{ km s}^{-1}$ ), for which we simply take the tabulated distances (with  $H_0 = 75 \text{ km s}^{-1} \text{ Mpc}^{-1}$ ).

It is known that in the vicinity of prominent overdensities the redshift-distance relation can become non-monotonic, such that there are three different distances corresponding to a given redshift (see the S-shaped curve of Fig. 14a in the following section). This makes ambiguous the distance assignments for the galaxies which fall in these triple-valued regions.

We treat as triple-valued zone objects also the field galaxies and the groups which would fall in these zones, if their redshifts were modified by  $\pm 100 \text{ km s}^{-1}$  and by a value equal to the group velocity dispersion, respectively. We calculate the velocity dispersions of groups using the robust scale estimator defined in terms of the "median absolute deviation" (Beers, Flynn & Gebhardt, 1990). In our cases all triple-valued zone field galaxies are spirals.

In practice, if we take the modified cluster dipole model, this problem concerns only 4 groups and 14 field galaxies in the Virgo region. If we take the attractor model relative to the Mark II subsample, this concerns 10 groups and 28 field galaxies located in the Virgo or GA regions. For the attractor model fitting the Mark III spirals, the redshift-distance relation remains monotonic in the vicinity of GA and there are 10 field galaxies (and the Virgo cluster) located in the triple-values regions of Virgo or PP.

In order to solve this problem, Tully & Shaya (1984) simply relied on some DIs, optical appearance, and connection with some Virgo clouds to guess the distance of the Virgo triple-valued zone galaxies. Yahil et al. (1991) used a distance-averaging procedure, which however, tends to place all objects in the middle branch of the triple-valued

zone; on the other hand, iteration schemes for translating from redshift space to distance space tend to place objects outside the middle branch (Yahil et al., 1991; Hudson, 1993a). Sigad et al. (1998) used a statistical approach which takes into account prior information on the peculiar velocity field.

We use the following precepts to solve the problem of the triple-valued zones. If a galaxy which falls in these zones is included in Mark III, among the three possible distances we choose that which is closer to the value given by Mark III. If a spiral galaxy is not included in Mark III, but has known apparent magnitude  $B_T$  and known maximum rotational velocity  $V_m$ , we can evaluate the three values of the absolute magnitude

$$M_B - 5 \log h = B_T - 5 \log r - 15.62 \quad (8)$$

which correspond to the three choices of distance  $r$  (expressed in  $\text{km s}^{-1}$ ). Then we compare the values of  $V_m$  and the three values of  $M_B - 5 \log h$  with the TF relation calibrated on a sample of galaxies lying at similar redshift, but outside the triple-valued zone. More precisely, for the calibration of the TF relation expressed as the linear relation

$$M_B - 5 \log h = a - b \log V_m \quad (9)$$

(with  $V_m$  in  $\text{km s}^{-1}$ ), we consider a sample consisting of all the galaxies which lie in a distance shell centered on the attractor, with the shell having the same width in distance as the distance range in which the redshift-distance relation is not monotonic. We find the TF relation by means of a regression analysis in which we calculate the ordinary least-squares bisector line, excluding iteratively the points which depart by  $3\sigma$  from the best regression line. After having derived the TF relation, for a galaxy located in the triple-valued zone we choose the distance which implies a value for the absolute magnitude closer to the TF relation.

We wish to point out that in this procedure we do not want to find the "true" TF relation to be used as an unbiased DI with low magnitude scatter; we simply use the TF as a criterium for choosing the distance of a triple-valued zone object, which is found only in restricted volumes close to prominent gravitational sources. In these circumstances systematic biases act in the same way on all galaxies and therefore should not affect our distance choices.

Table 7 reports the parameters of the TF relations (slope  $b$ , zero-point  $a$ , rms scatter  $\sigma$  (in mag)) we used for various regions and the three aforementioned peculiar velocity models. The slopes are in substantial agreement with the typical values ( $b \sim 5-6$ ) reported in the literature for blue TF relations (e.g., Tully & Fisher, 1977; Bottinelli et al., 1983; Garcia et al., 1993). As is expected, the rms scatters  $\sigma$  about the mean relations tend to be larger than the typical value of  $\sigma \sim 0.5 - 0.6$  mag for blue TF relations (Tully & Fisher, 1977), because of errors with which velocity field models reproduce the distance, and, especially, because of the inclusion in the sample of objects with inaccurate photometric and line width data (e.g., galaxies with uncertain inclination corrections of the 21 cm line widths).

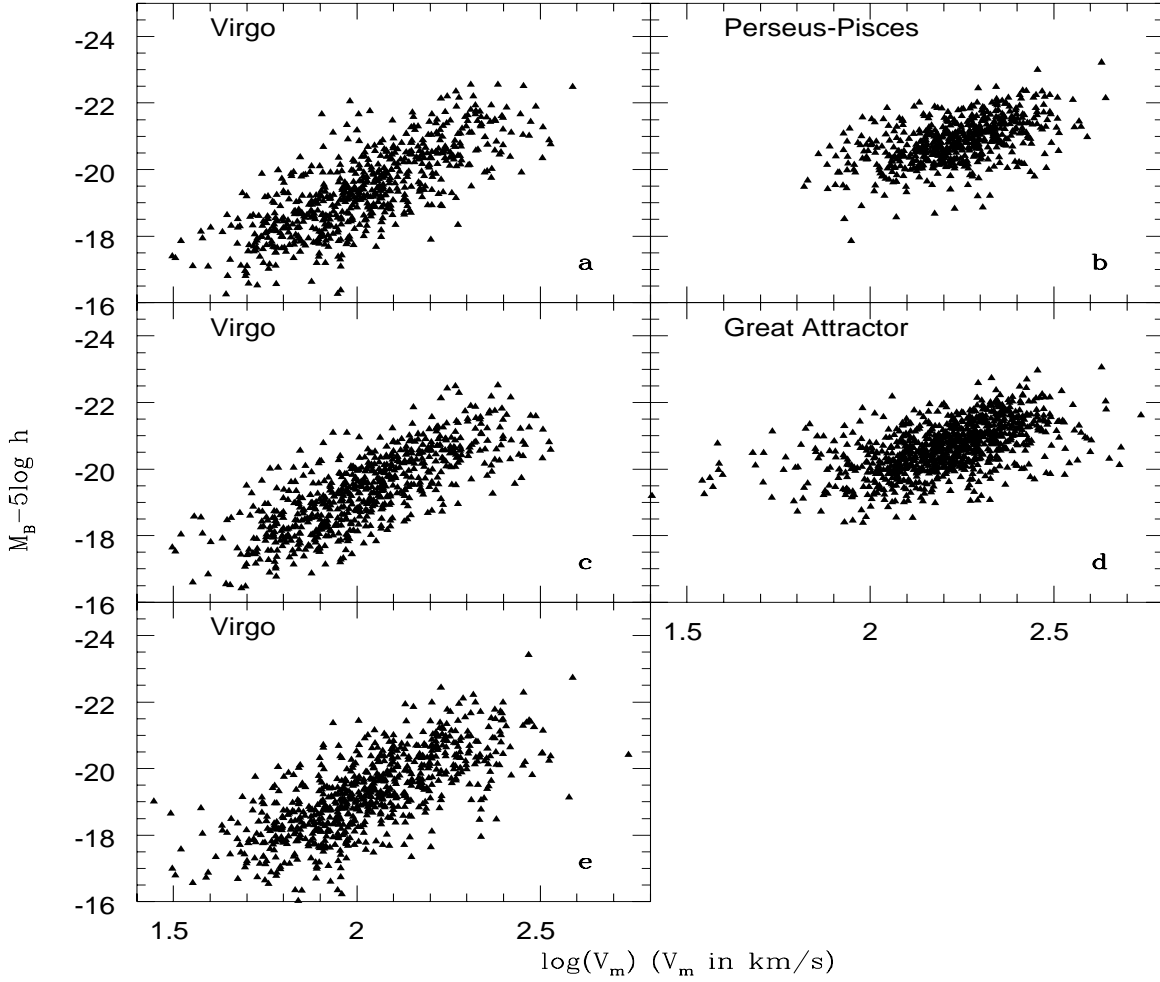


Fig. 13.— Plots of  $M_B - 5 \log h$  (where  $M_B$  is the blue absolute magnitude) versus  $\log V_m$  (where  $V_m$  is the maximum rotation velocity expressed in  $\text{km s}^{-1}$ ) for the galaxies located in the Virgo redshift region (e), (with galaxy distances predicted by the modified cluster dipole model), for the galaxies located in the Virgo (c) and GA (d) redshift regions (with galaxy distances predicted by the model fitted to the Mark II subset), for the galaxies located in the Virgo (a) and Perseus-Pisces (b) redshift regions (with galaxy distances predicted by the model fitted to the Mark III spirals).

The substantial reliability of the velocity field models considered is supported by the fact that they in general imply reasonable TF relations.

Fig. 13 shows the  $M_B - 5 \log h$  versus  $\log V_m$  plots for galaxies located in various redshift intervals corresponding to the triple-valued zones, with distances predicted by

different velocity models.

If we had also field ellipticals (which we do not have) lying in the triple-valued zones, we could have followed a similar procedure, using the modified Faber-Jackson relation instead of the TF relation. Remarkably, for the few triple-valued zone objects included in Mark III, our

TABLE 7  
THE PARAMETERS OF THE TULLY-FISHER RELATION.

Model	Region	N	a	b	$\sigma(\text{mag})$
Multi-attractor (Mark III*)	Virgo	641	$-6.70 \pm 0.35$	$6.27 \pm 0.16$	0.83
Multi-attractor (Mark II*)	Virgo	665	$-7.34 \pm 0.32$	$5.93 \pm 0.25$	0.79
Modified cluster dipole model	Virgo	743	$-7.28 \pm 0.40$	$5.87 \pm 0.20$	0.94
Multi-attractor (Mark III*)	PP	580	$-11.66 \pm 0.46$	$4.11 \pm 0.21$	0.63
Multi-attractor (Mark II*)	GA	957	$-13.15 \pm 0.38$	$3.39 \pm 0.18$	0.70

method for choosing the best distance yields the distance closer to the value tabulated in Mark III.

## 5 COMPARING THE RESULTS RELATIVE TO DIFFERENT VELOCITY FIELD MODELS

In Fig. 14 we show the predicted behaviors of the recession velocity and peculiar velocity against the distance from the attractor center, along the lines of sight of Virgo, GA, and PP. We also show the behavior of the peculiar velocity along the line of sight of SH. Fig. 14 and the previous Figs. 1, 2, 4, 5, well illustrate the main differences

between the models.

There are outstanding features common to the velocity field models considered, such as the presence of the attractors Virgo, GA, PP and SH; but their prominence appreciably differs among the models (see the above-mentioned plots and §3.2.2).

Notwithstanding the simple geometry adopted for the attractors, our multi-attractor model fitted on Mark III data delineates a complex velocity field, which well resembles the Mark III–POTENT velocity field presented by Dekel (1994, 1997), except for the Coma supercluster region.

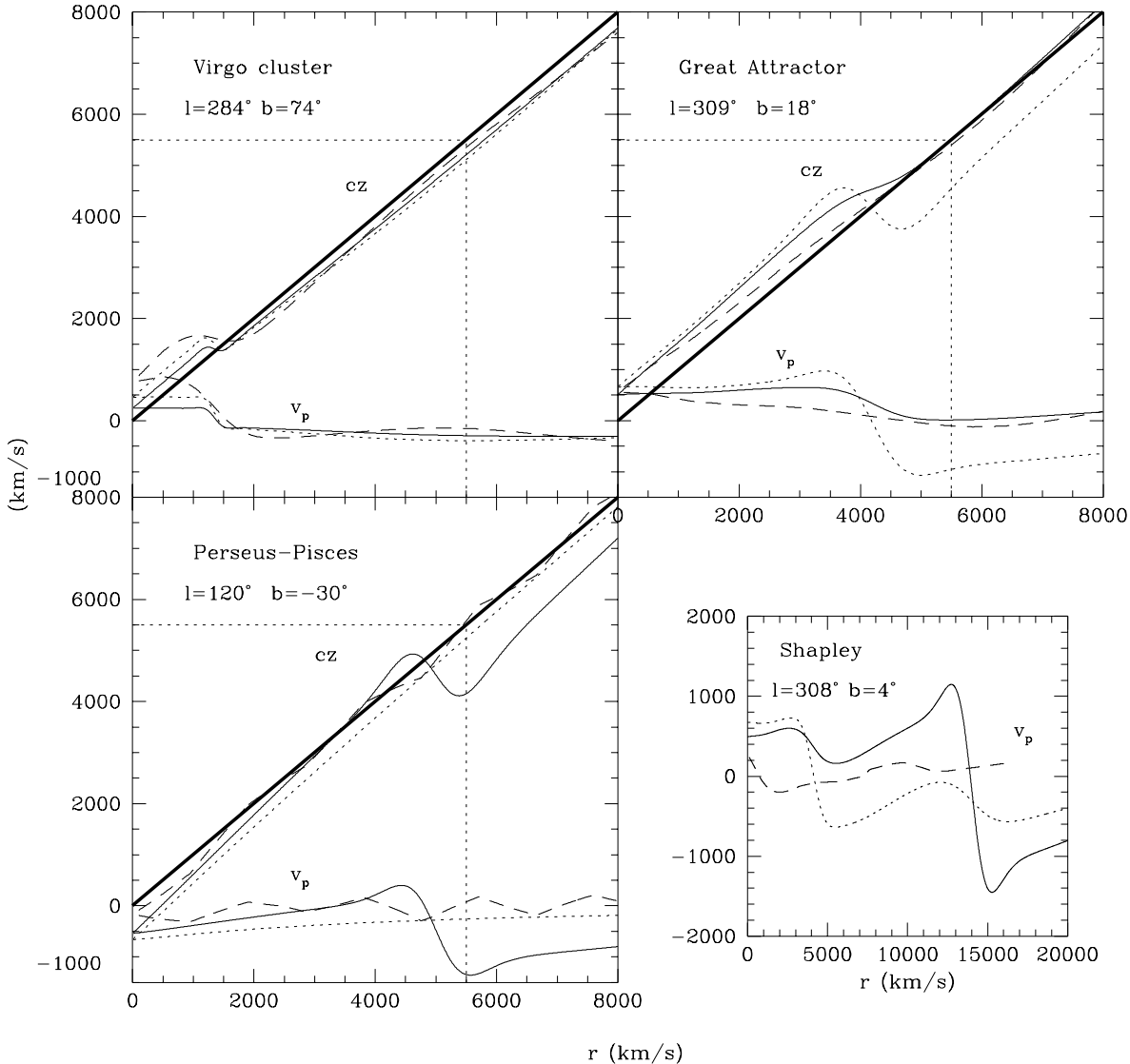


Fig. 14.— These plots present the behaviors of the recession velocity  $cz$  and peculiar velocity  $v_p$  (in the CMB frame), as predicted by some models of the peculiar velocity field, against the distance  $r$  (in  $\text{km s}^{-1}$ ) from the attractor center, along the lines of sight of Virgo ( $l = 284^\circ$ ,  $b = 74^\circ$ ), Great Attractor ( $l = 309^\circ$ ,  $b = 18^\circ$ ), and Perseus-Pisces ( $l = 120^\circ$ ,  $b = -30^\circ$ ). We also show the behavior of the peculiar velocity along the line of sight of the Shapley concentration ( $l = 308^\circ$ ,  $b = 4^\circ$ ). The dashed, dotted, and solid lines refer to the predictions of the modified cluster dipole model and multi-attractor models fitted to the Mark II subset and the whole Mark III, respectively. The Hubble relation  $cz = r$  is also indicated.

Compared to Mark II, Mark III gives particularly pronounced PP and SH attractors and a less dominant role for GA in shaping the velocity field. SH appears to account for nearly half the LG peculiar motion. Compared to the Mark III spirals, the velocity field of the whole Mark III, where E/S0 galaxies are included, is characterized by a greater region which is dynamically dominated by GA, but the value of  $\chi^2/dof$  and the errors on the model parameters are greater. In Mark III velocity maps there is no clear evidence of an infall pattern around PP, which rather acts in slowing down motions towards GA in the region comprised between LG and PP. On the other hand, large streaming flows in the general direction of the CMB apex are particularly remarkable.

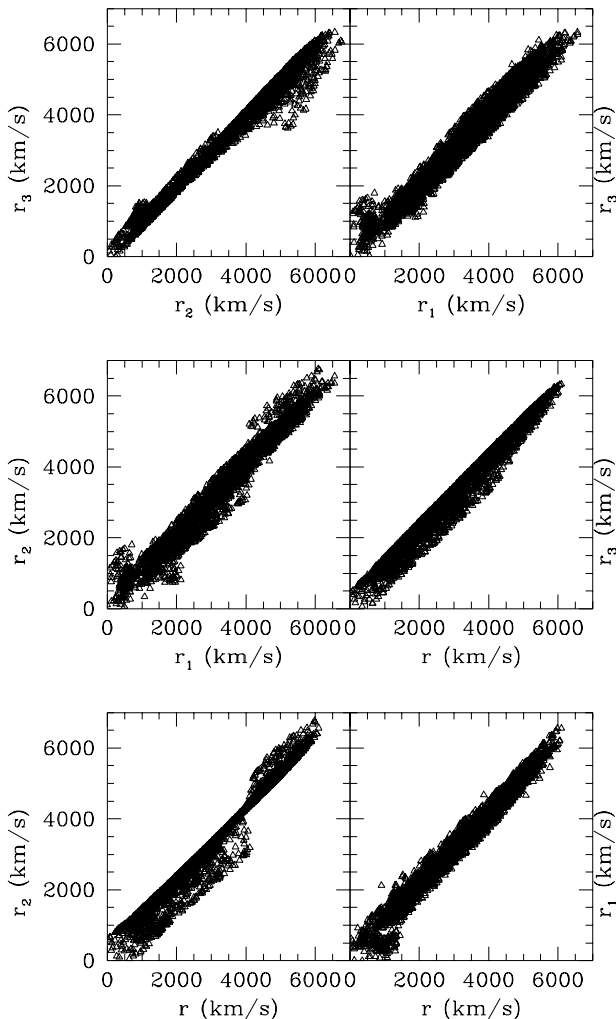


Fig. 15.— We show the comparisons between the uncorrected galaxy distance  $r = cz$  (expressed in  $\text{km s}^{-1}$  and in the CMB frame) and the three corrected galaxy distances (hereafter  $r_1$ ,  $r_2$ ,  $r_3$ ), as respectively predicted by the modified cluster dipole model, the multi-attractor models relative to the Mark II subsample and the Mark III spirals.

As regards the cluster dipole model, the reconstructed cluster density field (smoothed with a 1500

$\text{km s}^{-1}$  gaussian window) appears to be in satisfactory agreement with the Mark III POTENT density field in the nearby region ( $cz < 5000 \text{ km s}^{-1}$ ) of the supergalactic plane, where the GA and PP superclusters appear as prominent density peaks separated by an extended underdense region (see Plionis et al., 1996). There is less agreement in farther regions (just where peculiar velocity data are less reliable) so much that the Coma supercluster is replaced in Mark III POTENT density maps by an overdense region located in a displaced position. The corresponding velocity field maps bear less similarity than the density field maps, because the modified cluster dipole model is characterized by a well-defined infall pattern around PP, small large scale flows towards GA and SH, and large Virgo infall velocities in the local region. This large infall, which is at variance with most recent relevant estimates (see end of §3.1.2), enhances the flows towards GA in the LS region and makes the infall pattern around Coma almost disappearing. Thus, this large Virgo-centric infall makes the modified cluster dipole model less dissimilar from the Mark III multi-attractor model in the LS region than the original cluster dipole model.

Notably, the picture which is emerging from the application of the POTENT machinery to the new data of an ongoing peculiar velocity survey, the I-band TF distance survey of about 2000 spiral galaxies in the field (the SFI survey) and in the direction of 24 clusters (the SCI survey) (Giovannelli et al., 1997 a,b), bears some features which are seen in the modified cluster dipole model, such as a clear infall pattern around PP and the absence of coherent streaming flows on large scale (da Costa et al., 1996).

Differences in peculiar velocity models give rise to differences in the predicted galaxy distances. Fig. 15 shows the comparisons between the uncorrected distance  $r = cz$  and the three corrected distances (hereafter  $r_1$ ,  $r_2$ ,  $r_3$ ) we derive for all field galaxies and groups of our sample, as respectively predicted by the modified cluster dipole model, the multi-attractor models relative to the Mark II subsample and the Mark III spirals. The  $r_3$  versus  $r_1$  plot reveals a poor correlation especially at low values, where  $r_3 > r_1$  in many cases (mostly because of the large Virgo infall velocity which characterizes the first model). The  $r_2$  versus  $r_1$  plot reveals a poor correlation also at high values, mostly because of strong differences in the infall towards GA. The  $r_3$  versus  $r_2$  plot shows pronounced deviations from the one-to-one relation at low values ( $r_2 < 2000 \text{ km s}^{-1}$ ), where  $r_2 < r_3$  in many cases (mostly because of differences in the predicted Virgo-centric infall) and at high values ( $r_2 > 4000 \text{ km s}^{-1}$ ), where  $r_2 > r_3$  for many objects (mostly because of the smaller back-side infall towards GA given by Mark III with respect to Mark II). But this plot displays, on average, a smaller scatter than the two aforementioned diagrams, especially at low and intermediate values. The comparison between corrected and uncorrected distances shows that in general corrections are more important at low values, as expected; however, the  $r_2$  versus  $r$  plot displays a large scatter and marked systematic effects also at great values.

## 6 CONCLUSIONS

In this paper we provide homogeneous estimates of distances for the individual 3689 galaxies and the 485 groups (which contain a total of 2703 galaxies) of a large all-sky optical galaxy sample (Garcia et al., 1993; Garcia, 1993), which is limited to a depth of  $5500 \text{ km s}^{-1}$  and to the magnitude limit of completeness of  $B_T = 14 \text{ mag}$  (for  $|b| > 20^\circ$ ). This is the widest, complete, all-sky optical galaxy sample for which refined galaxy distances are available. All our distance estimates are available on request.

We recover the distances of our objects by correcting redshift-distances for peculiar motions through the application of some peculiar velocity field models.

We invert the distance-redshift relations relative to different velocity models and solve the problem of the triple-valued zones of this relation by using blue Tully-Fisher relations calibrated on suitably defined samples of objects having distances predicted by peculiar velocity models.

In our work we avoid taking inhomogeneous redshift-independent distances obtained from various classical DIs. Homogeneous redshift-independent distances are available for limited samples of galaxies and it is notoriously difficult to combine together the results coming from different DIs to achieve an uniform scale of distance. Moreover, we do not attempt to correct redshift-distances by using the peculiar velocity field derived from the positions and redshift of the galaxy sample itself, because this involves delicate strategies to recover the galaxy distribution in the unsampled zone of avoidance and because our galaxy sample does not include all the relevant gravitational sources for local peculiar motions.

We regard the peculiar velocity models considered as representative of current common views on the kinematics of cosmic flows in the nearby universe. However, refinements of the proper calibration of the Mark III Tully-Fisher relations, on which our velocity field models depend, are possible.

This point was raised by Davis, Nusser & Willick (1996). The authors performed a mode-by-mode comparison of the peculiar velocity fields expressed in sets of independent basis functions, that were fitted in redshift space to the inverse Tully-Fisher data from Mark III and to the predictions based on the  $1.2 \text{ Jy}$  IRAS density field (Fisher et al., 1995). Their best-fitting value of  $\beta \sim 0.6$  yielded no acceptable agreement between the two velocity fields within a region of  $6000 \text{ km s}^{-1}$  radius. On the other hand, using a new method, called VELMOD, for maximizing the likelihood of the Tully-Fisher observables, Willick et al. (1997b) found that the IRAS-predicted velocity field provided a satisfactory fit (with  $\beta \sim 0.5$ ) to the Mark III Tully-Fisher data, within  $3000 \text{ km s}^{-1}$  and on a small smoothing scale of  $300 \text{ km s}^{-1}$ , if one added an external quadrupole, which was essentially expected from the way in which the density field was smoothed. The discrepancy between these two approaches in comparing velocity fields might be a result of systematic errors incurred in matching the Mark III data subsets, an effect to which the latter

approach is insensitive.

Very recently, Willick & Strauss (1998) applied an implemented version of the VELMOD method to an expanded sample which comprises nearly all Mark III non-cluster spirals to  $7500 \text{ km s}^{-1}$ . The authors confirmed that the IRAS-predicted velocity field, with quadrupole, was a good fit to the Tully-Fisher data of that sample, for  $\beta \sim 0.5$  and smoothing scales of  $300$  or  $500 \text{ km s}^{-1}$ . But they recognized that the VELMOD Tully-Fisher calibration differed significantly from the Mark III Tully-Fisher calibration for the relatively distant ( $cz > 3000 \text{ km s}^{-1}$ ) galaxies of the WCF subsample, which covers particularly the region of the Perseus-Pisces supercluster. For these objects, the VELMOD Tully-Fisher relations, which, however, rely on the accuracy of the IRAS-predicted peculiar velocities, yield distances  $\sim 8\%$  shorter than the Mark III calibrations. The main effect is a reduction of the infall of the Perseus-Pisces region and, hence, of the bulk flow.

Ongoing observations aimed at giving reliable North-South homogenization (e.g., Strauss, 1997) will cast light on doubts concerning the validity of the Mark III Tully-Fisher calibration.

Certainly, major developments in peculiar velocity studies will arise by the turn of this century from analyses of peculiar velocity catalogs with data of superior quality (in terms of sky coverage, accuracy, and homogeneity), which can come out from peculiar velocity surveys in progress, based on the surface brightness fluctuation (Tonry et al., 1997), Type Ia supernovae (e.g., Riess et al., 1997), I-band Tully-Fisher (e.g., the SCI and SFI samples by Giovanelli et al., 1997a, b), and elliptical fundamental plane (e.g., Jørgensen, Franx & Kjaergaard, 1996; Wegner et al., 1996; Saglia et al., 1997) methods. New corrections to galaxy distances for peculiar motions can be easily implemented with the aid of some techniques used in this paper.

In any case, the use of different models of the peculiar velocity field allows us to check to what extent differences in the current views on the cosmic flows affect the recovering of galaxy distances in the nearby universe. We find that differences among distance estimates appear to be less pronounced in the  $\sim 2000\text{-}4000 \text{ km s}^{-1}$  distance range than in farther or nearer regions (see end of §5).

These differences can affect the optical luminosity function of a galaxy sample restricted to a fairly narrow solid angle. For instance, the addition of a Virgo infall alone of a few hundred km/s can brighten the characteristic magnitude  $M^*$  of the Schechter-type luminosity function by a few tenths of magnitude, for a shallow galaxy sample (e.g., Efstathiou, Ellis & Peterson, 1988). However, it can be proved that these differences have a small effect on the optical galaxy luminosity function of galaxy samples which, like our sample, cover a very large solid angle (see Marinoni et al. 1998b for a detailed discussion).

In general, peculiar velocity gradients are not strong so that all galaxies of a given region share similar peculiar motions. But in many regions of the nearby universe positive (or negative) peculiar radial velocities of a few hundred km/s are present; in these regions our corrections to galaxy

distances draw the objects which are nearby in angular position closer to each other (or farther from each other) by a few Mpc with respect to their uncorrected spatial locations. Remarkably, this effect has a minor impact on the local galaxy density on large scales (i.e., greater than a few Mpc), whilst it affects seriously the local galaxy density on small scales (i. e., roughly smaller than 1 Mpc) (see, e.g., Marinoni et al., 1998a for a preliminary account). Moreover, particularly in the above-mentioned nearest and farthest regions of the volume considered, the latter density parameter will be particularly sensitive to differences between the various sets of corrected distances.

The local galaxy density on small scales is an important parameter to be used in statistical studies of environmental effects on the properties of nearby galaxies, since it provides a well-defined characterization of galactic environment irrespective of membership in galaxy systems.

Remarkably, much of the observed evolution of the properties and populations of galaxies which has occurred during recent epochs ( $z < 1$ ) can be ascribed to interaction of galaxies and their local surroundings.

The authors are indebted to D. Burstein for his electronic distribution of the Mark II and Mark III datasets, A. M. Garcia for her electronic distribution of the data of her galaxy sample, E. Branchini and M. Plionis, who provided detailed results of their computations.

The authors would like to thank S. Bardelli, F. Mardirossian, and M. Mezzetti for useful conversations.

One of the authors (P. M.) has been supported by the EC TMR grant ERB4001GT962279.

This work has been partially supported by the Italian Ministry of University, Scientific and Technological Research (MURST) and by the Italian Space Agency (ASI).

## REFERENCES

- Aaronson, M., Bothun, G., Cornell, M. E. et al., 1989, *ApJ*, 338, 654.
- Aaronson, M., Huchra, J., Mould, J., Schechter, P. L., Tully, R. B., 1982 *ApJ*, 258, 64.
- Abell, G. O., 1958, *ApJS*, 3, 211.
- Abell, G. O., Corwin, H. G., Olowin, R. P., 1989, *ApJS*, 70, 1.
- Bardelli, S. et al., 1994, *MNRAS*, 267, 665.
- Beers, T. C., Flynn, K. & Gebhardt, K., *AJ*, 100, 32.
- Bertschinger, E. & Dekel, A., 1989, *ApJ*, 336, L5.
- Bottinelli, L., Gouguenheim, L., Paturel, G. & de Vaucouleurs, G., 1983, *A&A*, 118, 4.
- Branchini, E. & Plionis, M., 1996, *ApJ*, 460, 569 (BP96).
- Branchini, E., Plionis, M., & Sciama, D. W. 1996, *ApJ*, 461, L17.
- Burstein, D., 1989, The Mark II Catalog of Galaxy Peculiar Velocities (electronically distributed).
- Burstein, D., 1990, *Rep. Prog. Phys.*, 53, 421.
- Burstein, D., Davies, R.L., Dressler, A., Faber, S. M., Lynden-Bell, D., Terlevich, R. J., & Wegner, G. 1986, in *Galaxy Distances and Deviations from Universal Expansion*, eds. B. F. Madore & R. B. Tully (Boston: Reidel), 123.
- Corwin, H. G. & Skiff, B. A., 1998, *Extension to the Southern Galaxies Catalogue*, in preparation (ESGC).
- Courteau, S., 1992, Ph.D. Thesis, Univ. of California, Santa Cruz.
- Courteau, S., 1996, *ApJS*, 103, 363.
- Courteau, S., Faber, S. M., Dressler, A., & Willick, J. A. 1993, *ApJ*, 412, L51.
- da Costa, L. N. et al., 1996, *ApJ*, 468, L5.
- da Costa, L. N., Nusser, A., Freudling, W., Giovanelli, R., Haynes, M., Salzer, J. & Wegner, G., 1998, *MNRAS*, in press.
- Davis, M., Nusser, A. & Willick, 1996, *ApJ*, 473, 22.
- Davis, M. & Peebles, P. J. E., 1983, *ARA&A*, 21, 109.
- Dekel A., 1994, *ARA&A*, 32, 371.
- Dekel, A., 1997, in *Galaxy Scaling Relations: Origin, Evolution and Applications*, eds. L. da Costa & A. Renzini (Springer Verlag: Berlin), 245.
- Dekel, A., Bertschinger, E., Yahil, A., Strauss, M. A., Davis, M. & Huchra, J. P., 1993, *ApJ*, 412, 1.
- Dekel, A., Burstein, D. & White, S., 1997, in *Critical Dialogues in Cosmology*, ed. N. Turok (Singapore: World Scientific).
- de Vaucouleurs, G., & Bollinger, G., 1979, *ApJ*, 233, 433.
- de Vaucouleurs, G. & Peters, W. L., 1984, *ApJ*, 287, 1.
- de Vaucouleurs, G., de Vaucouleurs, A., Corwin, H. G et al., 1991, *Third Reference Catalogue of Bright Galaxies* (New York: Springer Verlag).
- Dressler, A. & Faber, S. M., 1990, *ApJ*, 354, 13.
- Dressler, A., Faber, S. M., Burstein, D., Davies, R. L., Lynden-Bell, D., Terlevich, R. J., & Wegner, G. 1987, *ApJ*, 313, L37.
- Efstathiou, G., Ellis, R. S. & Peterson, B. A., 1988, *MNRAS*, 232, 431.
- Ettori, S., Fabian, A. C. & White, D. A., 1997, *MNRAS*, 289, 787.
- Faber, S. M. & Burstein, D., 1988, in *Large-Scale Motions in the Universe*, eds. V.C. Rubin & G. V. Coyne, S. J (Princeton: Princeton University Press).
- Faber, S., Wegner, G., Burstein, D., Davies, R. L., Dressler, A., Lynden-Bell, D. & Terlevich, R. J., 1989, *ApJS*, 69, 763.
- Fisher, J. R. & Tully, R. B., 1981, *ApJS*, 47, 139.
- Fisher, K. B., Huchra, J. P., Strauss, M. A. et al., 1995, *ApJS*, 100, 69.
- Garcia, A. M., 1993, *A&AS*, 100, 47.
- Garcia, A. M., Paturel, G., Bottinelli, L. & Gouguenheim, L., 1993, *A&AS*, 98, 7.
- Giovanelli, R., Haynes, M., Herter, T., Vogt, N., da Costa, L., Freudling, W., Salzer, J. & Wegner, G., 1997a, *AJ*, 113, 22.
- Giovanelli, R., Haynes, M., Herter, T., Vogt, N., da Costa, L., Freudling, W., Salzer, J. & Wegner, G., 1997b, *AJ*, 113, 53.
- Girardi, M., Giuricin, G., Mardirossian, F., Mezzetti, M., Boschini, W., 1998, *ApJ*, in press.
- Giuricin, G., Limboz Tektunali F., Monaco, P., Mardirossian, F., Mezzetti, M., 1995, *ApJ*, 450, 41.
- Giuricin, G., Mardirossian, F., Mezzetti, M. & P. Monaco, 1993, *ApJ*, 407, 22.
- Giuricin, G., Monaco, P., Mardirossian, F., Mezzetti, M., 1994, *ApJ*, 425, 450.
- Gudehus, D., 1995, *A&A*, 302, 21.
- Han, M. & Mould, J. R. 1990, *ApJ*, 360, 448.
- Han, M. & Mould, J. R., 1992, *ApJ*, 396, 453.
- Huchra, J. P. & Geller, M., 1982, *ApJ*, 257, 423.
- Hudson, M. J., 1993a, *MNRAS*, 265, 43.
- Hudson, M. J., 1993b, *MNRAS*, 265, 72.
- Hudson, M. J., 1994a, *MNRAS*, 266, 468.
- Hudson, M. J., 1994b, *MNRAS*, 266, 475.
- Hudson, M. J., Dekel, A., Courteau, S., Faber, S. M. & Willick, J. A., 1995, *MNRAS*, 274, 305.
- Jørgensen, I., Franx, M. & Kjaergaard, P., 1996, *MNRAS*, 280, 167.
- Kaiser, N., Efstathiou, G., Ellis, R. et al., 1991, *MNRAS*, 252, 1.
- Kogut A. et al., 1993 *ApJ*, 419, 1.
- Kolatt, T., Dekel, A., Ganon, G., & Willick, J. A. 1996, *ApJ*, 468, 419.
- Kolokotronis, V., Plionis, M., Coles, P., Borgani, S. & Moscardini, L., 1996, *MNRAS*, 280, 186.
- Lahav, O., 1987, *MNRAS*, 225, 213.
- Lauberts, A., 1982, *The ESO-Uppsala Survey of the ESO (B) Atlas* (München: European Southern Observatory).
- Lauberts, A. & Valentijn, E., 1989, *The Surface Photometry Catalogue of the ESO-Uppsala Galaxies* (München: Euro-

- pean Southern Observatory).
- Lubin, P. & Vilella, M. P., *Ann. NY Acad. Sci.*, 470, 383.
- Lucey, J. R. & Carter, D., 1988, *MNRAS*, 235, 1177.
- Lynden-Bell, D., Faber, S. M., Burstein D., Davies, R. L., Dressler, A., Terlevich, R. J., & Wegner, G. 1988, *ApJ*, 326, 19.
- Marinoni, C., Giuricin, G., Costantini, B. & Monaco, P., 1998a, in *The Young Universe*, eds. D'Odorico S., Fontana, A. & Giallongo, E., *Astron. Soc. Pacific Conference Ser.*, San Francisco, California, in press.
- Marinoni, C., Monaco, P., Costantini, B., Giuricin, G., 1998b, in preparation.
- Materne, J., 1978, *A&A*, 63, 401.
- Mathewson, D. S., Ford, V. L., & Buchhorn, M., 1992 *ApJS*, 81, 413.
- Monaco, P., Giuricin, G., Mardirossian, F. & Mezzetti, M., 1994, *ApJ*, 436, 576.
- Nilson, P., 1973, *Uppsala General Catalogue of Galaxies*, Uppsala Astron. Obs. Ann., 6 (UGC).
- Nulsen, P. E. J. & Böhringer, H., 1995, *MNRAS*, 274, 1093.
- Peebles, P. J. E. 1980, *The Large Scale Structure of the Universe* (Princeton: Princeton Univ. Press).
- Plionis, M., Branchini, E., Zehavi, I., Dekel, A., 1996, in *Wide-Field Spectroscopy*, eds. Kontizas E. et al. (Dordrecht: Kluwer Academic Press), 311.
- Plionis, M. & Kolokotronis, V., 1998, in *Large-Scale Structure: Tracks and Traces*, eds. V. Müller et al. (Singapore: World Scientific), in press.
- Proust, D., Quintana, H. & Slezak, E., 1998, in *Large-Scale Structure: Tracks and Traces*, eds. V. Müller et al. (Singapore: World Scientific), in press.
- Quintana, H., Ramirez, A., Melnick, J., Raychaudhury, S. & Slezak, E., 1995, *AJ*, 110, 463.
- Raychaudury, S., Fabian, A. C., Edge, A. C., Jones, C. & Forman, W., 1991, *MNRAS*, 248, 101.
- Regös, E. & Geller, M. J., 1989, *AJ*, 98, 755.
- Reif, K., Mebold, U., Goss, W. M., Van Woerden, H. & Siegman, B., 1982, *A&AS*, 50, 451.
- Riess, A. G., Davis, M., Baker, J. & Kirschner, R. P., 1997, *ApJ*, 488, L1.
- Rowan-Robinson, M. et al., 1990, *MNRAS*, 247, 1.
- Saglia, R. P. et al., 1997, *ApJS*, 109, 79.
- Sandage, A. & Tamman, G. A., 1981, *A Revised Shapley-Ames Catalog of Bright Galaxies* (Washington: Carnegie Inst. of Washington) (RSA).
- Santiago, B. X., Strauss, M. A., Lahav, O. et al., 1995, *ApJ*, 446, 457.
- Santiago, B. X., Strauss, M. A., Lahav, O. et al., 1996, *ApJ*, 461, 38.
- Scaramella, R., Baiesi-Pillastrini, G., Chincarini, G., Vettolani, G. & Zamorani, G., 1989, *Nature*, 338, 562.
- Scaramella, R., Vettolani G., & Zamorani, G. 1991, *ApJ*, 376, L1.
- Shaya, E. J., Tully, R. B. & Pierce, M. J., 1992, *ApJ*, 391, 16.
- Shimasaku, K., & Okamura, S. 1992 *ApJ*, 398, 441.
- Sigad, Y., Eldar, A., Dekel, A., Strauss, M. & Yahil, A., 1998, *ApJ*, in press.
- Strauss, M. A., 1997, in *Critical Dialogues in Cosmology*, ed. N. Turok (Singapore: World Scientific), 423.
- Strauss, M. A., Davis, M., Yahil, A., & Huchra, J. P. 1992a, *ApJ*, 385, 421.
- Strauss, M. A., Huchra, J. P., Davis, M., Yahil, A., Fisher, K. B. & Tonry, J. P., 1992b, *ApJS*, 83, 29.
- Strauss, M. A. & Willick J. A., 1995, *Physics Reports*, 261, 271.
- Susperregi, M. & Buchert, T., 1997, *A&A*, 323, 295.
- Tonry, J. L., Blakeslee, J. P., Ajhar, E. A. & Dressler, A., *ApJ*, 475, 399.
- Tonry, J. L., & Davis, M., 1981, *ApJ*, 246, 680.
- Tonry, J. L et al., 1992, *BAAS*, 23, 1341.
- Tormen, B. & Burstein, D., 1995, *ApJS*, 96, 123.
- Tully, R. B., 1980, *ApJ*, 237, 390.
- Tully, R. B., 1987, *ApJ*, 321, 280.
- Tully, R. B., 1988a, *Nearby Galaxies Catalog* (Cambridge: Cambridge Univ. Press) (NBG).
- Tully, R. B., 1988b, *AJ*, 96, 73.
- Tully, R. B. & Fisher, J. R., 1977, *A&A*, 54, 661.
- Tully, R. B. & Fisher, J. R., 1987, *Nearby Galaxies Atlas* (Cambridge: Cambridge Univ. Press).
- Tully, R. B., & Shaya, E. J. 1984, *ApJ*, 281, 31.
- Vettolani, G., Chincarini, G., Scaramella, R. & Zamorani, G., 1990, *AJ*, 99, 1709.
- Wegner, G. et al., 1996, *ApJS*, 106, 1.
- Willick, J. 1990, *ApJ*, 351, L5.
- Willick, J., 1991, Ph. D. thesis, Univ. of California, Berkeley.
- Willick, J., 1994, *ApJS*, 92, 1.
- Willick, J. A., Courteau, S., Faber, S. M., Burstein, D. & Dekel, A., 1995, *ApJ*, 446, 12.
- Willick, J. A., Courteau, S., Faber, S. M., Burstein, D., Dekel, A., Kolatt, T. 1996, *ApJ*, 457, 460.
- Willick, J. A., Courteau, S., Faber, S. M., Burstein, D., Dekel, A., Strauss, M. A. 1997a, *ApJS*, 109, 333.
- Willick, J. A. & Strauss, M. A., 1998, *ApJ*, submitted.
- Willick, J. A., Strauss, M. A., Dekel, A. & Kolatt, T., 1997b, *ApJ*, 486, 629.
- Yahil, A., Sandage, A. & Tamman, G. A., 1977, *ApJ*, 217, 903.
- Yahil, A., Sandage, A. & Tamman, G. A., 1980, *ApJ*, 242, 448.
- Yahil, A., Strauss, M. A., Davis, M., & Huchra, J., 1991, *ApJ*, 372, 380.
- Zucca, E., Zamorani, G., Scaramella, R., Vettolani, G., 1993, *ApJ*, 407, 470.
- Zwicky, F. et al., 1961-1968, *Catalog of Galaxies and Clusters of Galaxies*, Vols. 1-6 (Pasadena: California Inst. of Technology) (CGCG).